Mycena genomes resolve the evolution of fungal bioluminescence

Huei-Mien Ke[1], Hsin-Han Lee[1], Chan-Yi Ivy Lin[1,2], Yu-Ching Liu[1], Min R. Lu[1,3], Jo-Wei Allison Hsieh[3,4], Chiung-Chih Chang[1,5], Pei-Hsuan Wu[6], Meiyeh Jade Lu[1], Jeng-Yi Li[1], Gaus Shang[7], Rita Jui-Hsien Lu[2,8], László G. Nagy[9], Pao-Yang Chen[3,4], Hsiao-Wei Kao[5] and Isheng Jason Tsai[1,3]

[1] Biodiversity Research Center, Academia Sinica, Taipei, Taiwan

[2] Department of Molecular, Cellular and Developmental Biology, Yale University, New Haven, Connecticut 06520, USA

[3] Genome and Systems Biology Degree Program, Academia Sinica and National Taiwan University, Taipei, Taiwan

[4] Institute of Plant and Microbial Biology, Academia Sinica, Taipei, Taiwan

[5] Department of Life Sciences, National Chung Hsing University, Taichung, Taiwan

[6] Master Program for Plant Medicine and Good Agricultural Practice, National Chung Hsing University, Taiwan

[7] Department of Biotechnology, Ming Chuan University, Taiwan

[8] Department of Medicine, Washington University in St. Louis, St. Louis, MO 63110, USA

[9] Synthetic and Systems Biology Unit, Biological Research Centre, 6726 Szeged, Hungary

Correspondence: Huei-Mien Ke cotton@sinica.edu.tw and Isheng Jason Tsai ijtsai@sinica.edu.tw

Abstract

Mushroom-forming fungi in the order Agaricales represent an independent origin of bioluminescence in the tree of life, yet the diversity, evolutionary history, and timing of the origin of fungal luciferases remain elusive. We sequenced the genomes and transcriptomes of five bonnet mushroom species (*Mycena* spp.), a diverse lineage comprising the majority of bioluminescent fungi. We show that bioluminescence evolved in the common ancestor of *Mycena* spp. and the marasmioid clade of Agaricales and was maintained through at least 160 million years of evolution. We revealed *Mycena* exhibit two-speed genomes and resolve how the luciferase cluster was derived by duplication and translocation, frequently rearranged and lost in most *Mycena* species, but conserved in the *Armillaria* lineage. Luciferase cluster members were co-expressed across developmental stages, with highest expression in fruiting body caps and stipes, suggesting fruiting-related adaptive functions. Our results contribute to understanding a *de novo* origin of bioluminescence and the corresponding gene cluster in a diverse group of enigmatic fungal species.

The genus *Mycena* (Pers.) Roussel, comprises approximately 600 small mushroom species widely distributed around the world[1]. Also known as bonnet mushrooms, *Mycena* species are usually characterised by a bell-shaped cap, a thin stem (**Fig. 1a**), and a gilled or porioid hymenophore[2]. *Mycena* also have a diversity of life history strategies; while many species are saprotrophic, they can be pathogens as well as mycorrhizal[3]. Despite its vast diversity of lifestyles and phenotypes, there are many outstanding questions concerning the basic biology, ecology and genomics of this genus. One particular fascinating trait is bioluminescence, which more than half of the 81 recorded luminescent fungi belong to *Mycena*[4]. Yet, bioluminescence occurs only in a small percentage of this genus, suggesting an intricate loss/gain history and potential convergence within the genus.

Fungal light emission involves two main steps. First, a luciferin precursor of hispidin is hydroxylated by hispidin-3-hydroxylase (H3H) into 3-hydroxyhispidin (luciferin)[5]. Oxygen is then added to the luciferin by luciferase, producing a high energy intermediate which is subsequently decomposed, yielding light emission. Previously, Kotlobady *et al.* have identified the fungal luciferase, which is physically adjacent to these enzymes and forms a gene cluster containing luciferase, hispidin synthase and H3H[6]. This cluster was found to be conserved across bioluminescent fungi of three lineages: *Armillaria*, mycenoid and *Omphalotus*[6]. Phylogeny reconstruction suggested that luciferase originated in early Agaricales. *Armillaria* and *Omphalotus* belong to the marasmioid clade, whereas *Mycena* was recently found to be sister of the marasmioid clade[7]. Recent genome sequencing efforts in the marasmioid clade revealed diverse genomic and life history traits, including genome expansion and pathogenicity in *Armillaria* spp.[8], novel wood decay strategies[9] or fruiting body development[10]. Genomes of two *Mycena* species were sequenced[6], however, the fragmented assemblies (N50 5.8–16.7 kb) impeded comparative genomic analyses of features such as synteny[11]. These resources provide a substrate for studies of genome evolution and of bioluminescence in fungi, however, several key questions are still unknown from an evolutionary perspective. Here, we set out to identify novel genes involved in bioluminescence, understand how the luciferase cluster was lost or retained, and whether there are levels of variation in this cluster across these lineages.

To gain insights into the evolution of fungal bioluminescence and the ecology of mycenoid, we sequenced the genomes of four bioluminescent (*Mycena chlorophos*, *M. kentingensis*, *M. sanguinolenta* and *M. venus*) and one non-bioluminescent (*M. indigotica*) species. We conducted comparative genomics with representative genomes of all bioluminescent fungal clades, putting particular emphasis on genome-wide

synteny to investigate the evolutionary dynamics of the luciferase gene cluster through hundreds of millions of years. The variability in genome sizes among *Mycena* is likely associated with the differential expansion of repeats in the genomes, potentially due to the differential control on repeat activity by DNA methylation. The transcriptome of bioluminescent mycelium correctly revealed the luciferase cluster and co-expression analyses identified further genes that may be relevant to bioluminescence and development. Based on comparative analyses from fifteen available genomes of bioluminescent fungi, we reconstructed and presented a model for evolution of fungal bioluminescence.

Results

Assemblies and annotations of five *Mycena* species

We sequenced the genomes of the bioluminescent fungi *Mycena chlorophos*, *M. kentingensis*, *M. sanguinolenta* and *M. venus,* as well as the non-bioluminescent *M. indigotica* (**Fig. 1a**). These species were chosen for their phylogenetic positions (Supplementary Fig. 1) and because they displayed different bioluminescence intensities. An assembly was produced for each species using a combination of Illumina and Oxford Nanopore reads (Supplementary Table 1). The nuclear genomes were 50.9–167.2 Mb with two amongst the largest for the Agaricales. The assemblies consisted of 30–155 contigs with N50 4.1–17.8 Mb (Supplementary Table 2), which were comparable to representative fungal reference assemblies and allowed for synteny comparisons[11]. Stretches of TTAGGG hexamers were identified at the end of scaffolds, indicating telomeric repeats commonly found in Agaricales[12,13]. The largest scaffolds in *M. indigotica* and *M. kentingensis* were telomere-to-telomere, indicating gapless chromosomes. Mitochondrial genomes in these species were assembled into single circular contigs of 88.3–133 kb (Supplementary Fig. 2).

Using a combination of reference fungal protein homology support and mycelium transcriptome sequencing (Supplementary Table 3), 13,940–26,334 protein encoding genes were predicted in the *Mycena* genomes using MAKER2[14] pipeline, and were 92.1–94.8% complete (Supplementary Table 2) based on BUSCO[15] analysis. Orthology inference using Orthofinder[16,17] placed these genes models and those of 37 other basidiomycetes genomes (Supplementary Table 4) into 22,244 orthologous groups (OGs; Supplementary Table 5). Of these OGs, 44.3% contained at least one orthologue from other basidiomycete, while 15–29% of the proteomes were found exclusively in each *Mycena* species (Supplementary Table 6). The genome sizes were positively correlated with proteome sizes, with the largest (*M. sanguinolenta*) and smallest (*M.*

chlorophos) varying two- and three-fold, respectively. Interestingly, the mitochondrial genomes were larger in species with smaller genomes, and this was due to various genes having gained an extensive number of introns (Supplementary Fig. 2). We assessed orthologous group evolution by analysing OG distribution dynamics along a time-calibrated phylogeny using CAFÉ[18]. Gene family changes were comparable to those of other branches of Agaricales. A total of 589 orthologous groups were expanded at the origin of the mycenoid lineage (Supplementary Fig. 3). Analysis of gene ontology terms showed that these genes were enriched in iron ion binding, transferase activity, DNA-binding transcription factor activity, and monooxygenase and dioxygenase activities, suggesting that these genes were necessary for mycenoid species adapting to different environments (Supplementary Table 7).

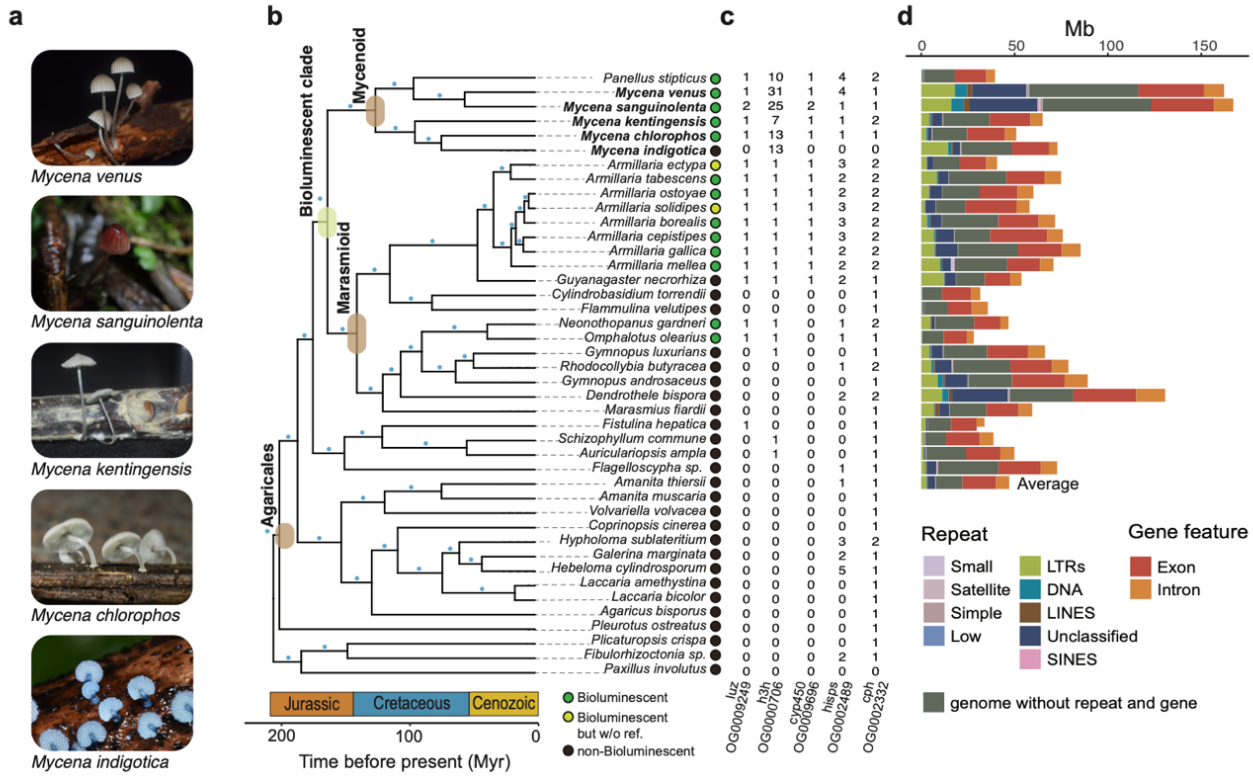

Fig. 1| Phylogenomic analysis of *Mycena* and related fungi. a, The five species sequenced in this study. **b**, Species trees inferred from a concatenated supermatrix of the gene alignments using the 360 single-copy orthogroups. X-axis denotes divergence time estimates. Blue dot on a branch indicates a bootstrap value > 90. **c**, Gene copy number in the orthologous groups (OG) associated with luciferin biosynthesis pathway including luciferase (*luz*), hispidin-3-hydroxylase (*h3h*), hispidin synthase (*hisps*), cytochrome P450 (*cyp450*) and caffeylpyruvate hydrolase (*cph*). **d**, Genome sizes for 42 species broken down by repeat types and gene features.

136 Averaged content in the genomes of 14 outgroup species are indicated as one bar. Repeats
137 including transposable elements (TEs): long terminal repeats (LTRs), long interspersed nuclear
138 elements (LINES), short interspersed nuclear elements (SINEs), DNA transposons (DNA), and
139 other types of repeats: small RNA (Small), simple repeats (Simple), and low complexity repeats
140 (Low).
141

142 **A single origin of bioluminescent fungi in the ancestor of *Mycena* and the**
143 **marasmioid clade**

144 Phylogenomic analyses based on single-copy orthologue sets have placed *Mycena*
145 sister to the marasmioid clade, including *Armillaria* and *Omphalotus*, which are the
146 other two lineages in which bioluminescent species have been identified. This species
147 phylogeny was recovered in both maximum likelihood analysis[19] of a concatenated
148 supermatrix of single-copy gene alignments (**Fig. 1b**) and coalescent-based analysis
149 using the 360 gene trees[20] (Supplementary Fig. 4). In our four bioluminescent *Mycena*
150 species, we identified genes involved in luciferin biosynthesis and their orthologues
151 across species (**Fig. 1c**). Phylogenies of individual gene families were congruent with
152 the species tree (Supplementary Fig. 5 (a–e). In contrast to a previous report[6], our
153 results suggest that the functional luciferase originated in the last common ancestor of
154 mycenoid and marasmioid clade rather than in that of the Agaricales (**Fig. 1b**). The
155 ancestral luciferase was initially duplicated in the last common ancestor of this large
156 group and Schizophyllaceae and subsequently acquired bioluminescence ability after
157 speciation (**Fig. 1c**; Supplementary Fig. 5a). Using MCMCtree[21] with three fossil
158 calibrations, we estimated the age of mycenoid most recent common ancestor to be
159 105–147 million years ago (Mya) in the Cretaceous (**Fig. 1b**). This is consistent with
160 recent estimates (78–110[7] and mean 125[1] Mya) and overlaps with the initial rise and
161 diversification of angiosperms[22], suggesting that they are ecologically associated with
162 fungi acting as saprotrophs or mycorrhizal partners[3]. Finally, the age of
163 bioluminescence which was also the age of functional luciferase in fungi was estimated
164 to originate around 160 million years ago during the late Jurassic (**Fig. 1b**).
165

166 **Interplay between transposable elements and DNA methylation in *Mycena***

167 Similar to other fungal genomes[23,24], much of the variation in the *Mycena* nuclear
168 genome can be explained by repetitive DNA content (Supplementary Table 8). Only
169 11.7% of the smallest genome (*M. chlorophos*) was repeats, which is in stark contrast
170 to the 39.0% and 35.7% in *M. sanguinolenta* and *M. venus*, respectively. The majority
171 of transposable elements in *Mycena* were long terminal repeats (LTRs) retrotransposons
172 (60–85%), followed by DNA transposable elements (11%–24%) (**Fig. 1d** and
173 Supplementary Table 8). Interestingly, the larger genomes of *M. sanguinolenta* and *M.*

venus contained the lowest proportion of LTRs (24.9 and 31.1%, respectively), but highest proportion of unclassified repeats (55.4 and 50.3%, respectively) (Supplementary Table 8). 16.6–36.5% of the unclassified repeat families shared 53.8–60.5% nucleotide identity with known transposable elements, suggesting they were degenerated copies which we defined as relic TEs (Supplementary Table 9). **Fig. 2a** shows that the largest assembled chromosome of *M. indigotica* exhibits high protein-coding gene content and low transposable element density at scaffold centres, which is typical of fungal chromosomes[25,26]. Such observations were consistent across large *Mycena* scaffolds (typically >1 Mb), suggesting that our assemblies were robust enough to capture evolutionary dynamics across chromosomes.

We detected DNA methylation levels of 5-methylcytosine (5mC) across the five *Mycena* assemblies using Nanopore long reads. CG sites were found either highly (mCG level >60%) or weakly methylated (<15%) in gene body, displaying a bimodal distribution (Supplementary Fig. 6). Such a bimodal distribution has also been observed in plants, animals, and other fungi, including *Tuber melanosporum* and *Pseudogymnoascus destructans*[27-32]. Within *Mycena*, the CG methylation in genes (5.4–10.5%) was much lower than that in repeats—i.e., TEs and unclassified repeats (11.6–84.5%) (**Fig. 2b**; Supplementary Table 10)—suggesting that DNA methylation may have a specific effect on repeats. Except for DNA transposons in *M. kentingensis*, LTR retrotransposons had the highest CG methylation levels of all types of transposable elements (**Fig. 2b**). Furthermore, CG methylation in relic TEs was clearly lower than that in classic TEs (Supplementary Table 10). Among the *Mycena* species, we found that *M. sanguinolenta* and *M. venus* with larger genomes and higher repeat content had lower levels of methylation in the repeats, and the repeat methylation was much higher in *M. indigotica*, *M. chlorophos*, and *M. kentingensis,* which have smaller genomes (**Fig. 2c**). The same pattern was also observed in genes, though they had fewer changes in their methylation level than did repeats. Our results indicate that the variant composition of repeats is differentially mediated by DNA methylation among closely-related *Mycena* species. Hence, genome expansion in *Mycena* was likely a result associated with transposable element proliferation and the accumulation of relic TEs, which yielded reduced methylation in active copies; this is also observed in some plants, e.g., *Arabis alpine*[33] and *Manihot esculenta*[34].

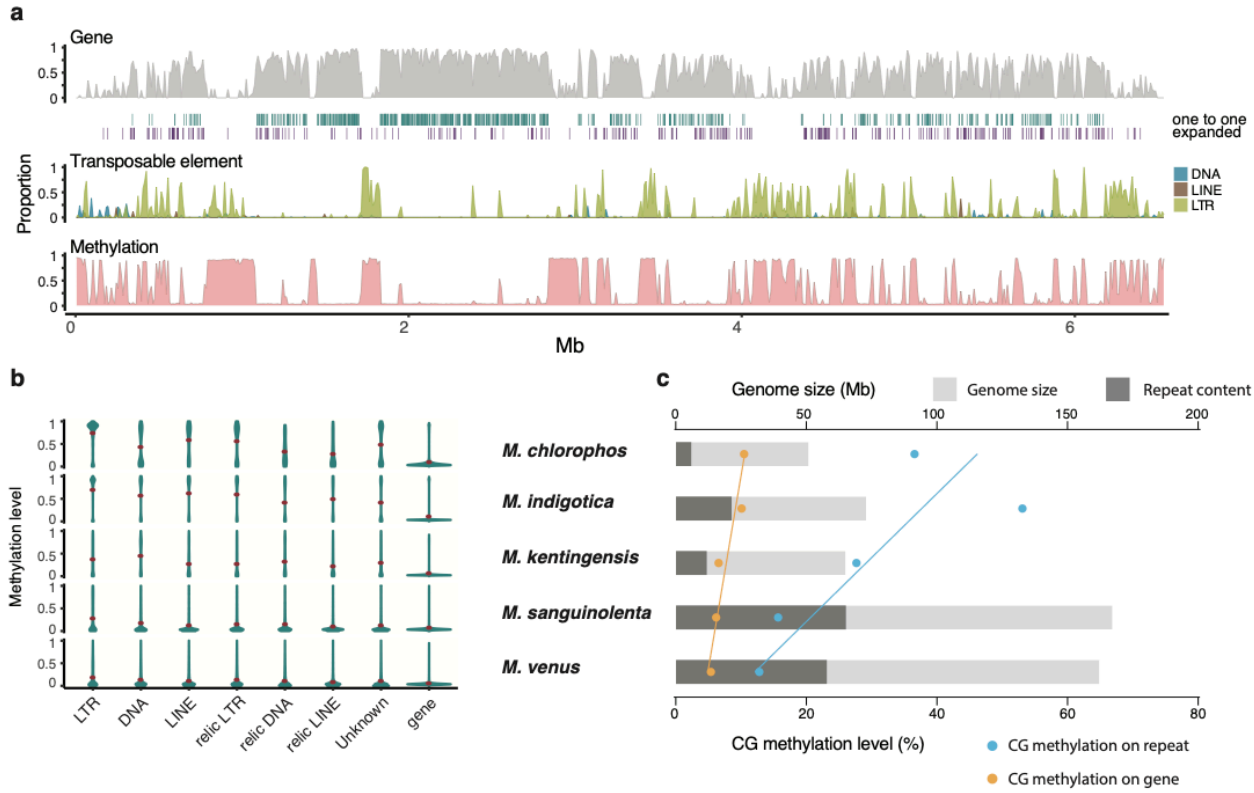

Fig. 2| Distribution of *Mycena* genome features. a, *M. indigotica* chromosome one. For every non-overlapping 10-kb window, the distributions from top to bottom are: (1) Gene density (percentage of nucleotides coverage). Stripes under this window denotes gene positions. Green stripe: gene containing single-copy orthologue with *M. chlorophos*. Purple stripe: gene expansion in individual species identified by CAFÉ. (2) Density of transposable elements (TEs), including LTRs, LINES, and DNA. (3) Average methylation level called from CpG sites per window. The high methylation window generally clustered in high TE regions with low gene density. **b**, The methylation level in genes and different types of repeats. **c**, The relationships among genome size, number of repeats and CG methylation levels in *Mycena*.

Core/dispensable genome partitioning based on synteny

We compared the patterns of 4,452 single-copy orthologue pairs between assemblies of *Mycena indigotica* and *Armillaria ectypa* (Supplementary Fig. 7). The majority of scaffolds between the two species were assigned to one-one relationship unambiguously, providing strong evidence that macro-synteny has been conserved between the marasmioid and mycenoid clades. There was no evidence of whole genome duplication events. Such chromosome-level synteny is also conserved in the common ancestor of Agaricales (Supplementary Fig. 8). The *M. indigotica* scaffolds typically exhibit high orthologous gene density in the centres of scaffolds **(Fig. 2a)**, and multi-genome comparison showed that synteny conservation was lost across the *Mycena* assemblies. Based on differential synteny exhibited across genomes, we further partitioned the scaffolds into core and dispensable regions (Methods). **Fig. 3a** shows that the core regions were typically at the scaffold centres of the *Mycena* species. In contrast, the dispensable regions can extend to a few mega-bases, even to entire scaffolds, as was the case for the largest (12.0 Mb) assembled scaffold of *M. venus* (**Fig. 3a**). These dispensable regions are highly enriched in repeats; they have a 3–8-fold higher methylation level and are overrepresented in expanded and contracted OGs compared to the core regions (**Fig 3b**; Supplementary Table 11; two-proportions z-test, $P < 2.2E-16$). Expansions and contractions were 3.5–6.7 and 2–3.5-fold higher in the dispensable regions, respectively. The observation that half the relative sequence coverage was independent to other scaffolds suggests that some of these dispensable scaffolds have aneuploidy (**Fig. 3c**). Two large scaffolds (>1Mb) displaying half the relative depth of coverage were present in *M. venus* (scaffold01; 12 Mb) and *M. sanguinolenta* (scaffold12; 4.5 Mb), both of which have larger genome sizes compared to other species. Interestingly, these scaffolds exhibit higher repeat content with reduced methylation level, as well as expanded proteins which resembles the lineage-specific chromosomes observed in some fungi[35]. For example, scaffold12 of *M. sanguinolenta* contains 32 copies of expanded ARD domain (PF03079) encoded by 31 proteins, which is involved in the methionine salvage pathway modulating cell division[36] (**Fig. 3d**). Together, these results suggest that some *Mycena* genomes possessed two-speed genomes similar to filamentous pathogenic fungi where genomes are compartmentalised into gene-dense and gene-sparse regions enriched in transposable elements[37]. Differential gain and loss of genes in the dispensable regions may have important implications for *Mycena*.

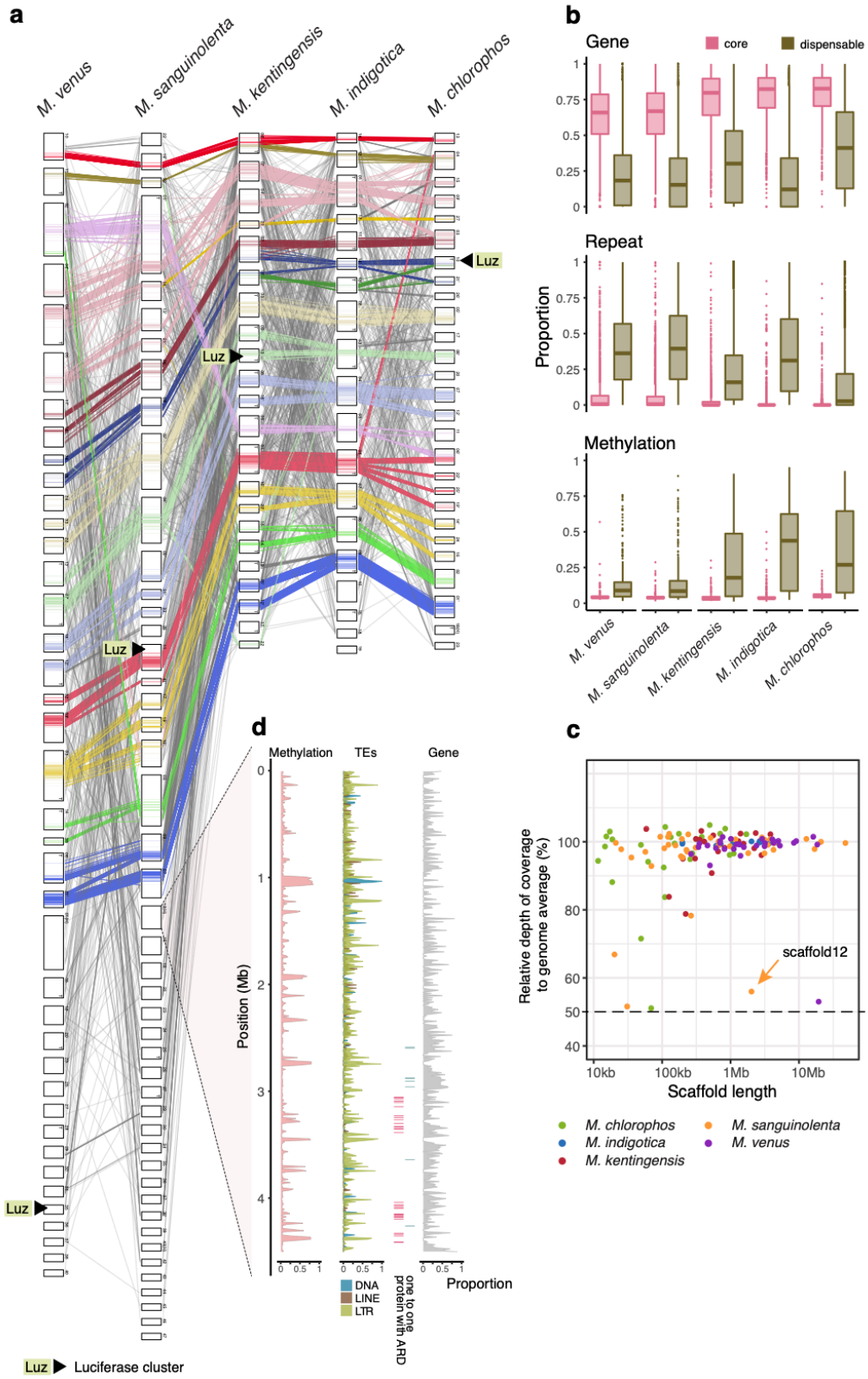
a
M. venus
M. sanguinolenta
M. kentingensis
M. indigotica
M. chlorophos
Luz
Luz
Luz
Luz
Luz ▶ Luciferase cluster
b
Gene
core
dispensable
Repeat
Methylation
Proportion
M. venus
M. sanguinolenta
M. kentingensis
M. indigotica
M. chlorophos
c
Relative depth of coverage to genome average (%)
scaffold12
Scaffold length
10kb
100kb
1Mb
10Mb
M. chlorophos
M. indigotica
M. kentingensis
M. sanguinolenta
M. venus
d
Methylation
TEs
Gene
Position (Mb)
DNA
LINE
LTR
one to one protein with ARD
Proportion

Fig. 3| The core and dispensable regions of scaffolds and anchoring for the four *Mycena* species scaffolds to *M. indigotica* reference genomes. a, Schematic representation of the inter-scaffold relationship between species. The links between scaffolds denoted the pairwise single-copy orthologues with closest related species. The core (coloured region in box) and dispensable regions in each scaffold were defined by the consecutive genes with less than 90 percent genetic distance to the adjacent one. The black triangle denotes the luciferase cluster. **b**, The gene density, repeat density and methylation level in core or dispensable regions. The gene and repeat densities are calculated from the non-overlapping 10-kb window located in the core or dispensable regions. The methylation level was calculated from the mean CG methylation level in core or dispensable regions. **c**, Sequence coverage was measured by the average number of reads that aligned to known reference bases per 10-kb non-overlapping windows with mosdepth[38]. Sequence coverage across scaffolds were normalized by the median coverage. The windows with more than 25% TEs were omitted. The coverage of each scaffold is normalized by the median coverage among the scaffolds longer than N90 in five species, except the Msan.scaffold36, which has 4-fold higher coverage than median coverage. **d,** Scaffold12 of *M. sanguinolenta* with expansion of proteins with the ARD domain. For every non-overlapping 10-kb window, the distribution from right to left is: (1) Density (percentage of nucleotides coverage) of gene. Green stripe denotes a gene containing single-copy orthologue with *M. venus*. Red stripe denotes the proteins with the ARD domain. (2) Density of transposable elements (TEs) including LTRs, LINES and DNA. (3) Average methylation level called from CpG sites per window.

Evolutionary dynamics of luciferase clusters

One of the previous challenges in addressing the evolution of fungal bioluminescence was that the bioluminescent species were scattered across the mycenoid and marasmioid clades, and this could only be explained by frequent loss of luciferase clusters. We used all the highly contiguous assemblies across the bioluminescent lineages in hand to investigate synteny around the luciferase cluster (**Fig. 4**). The genes surrounding the luciferase cluster among the eight *Armillaria* species generally shared the same order, but collinearity was partially lost in *G. necrorhiza* (**Fig. 4**). We reconstructed the ancestral upstream and downstream gene synteny of the *Armillaria* luciferase cluster and found that each belonged to different core regions of the same chromosome, suggesting that these regions were previously rearranged—including the luciferase cluster—and were subsequently retained (Supplementary Fig. 10).

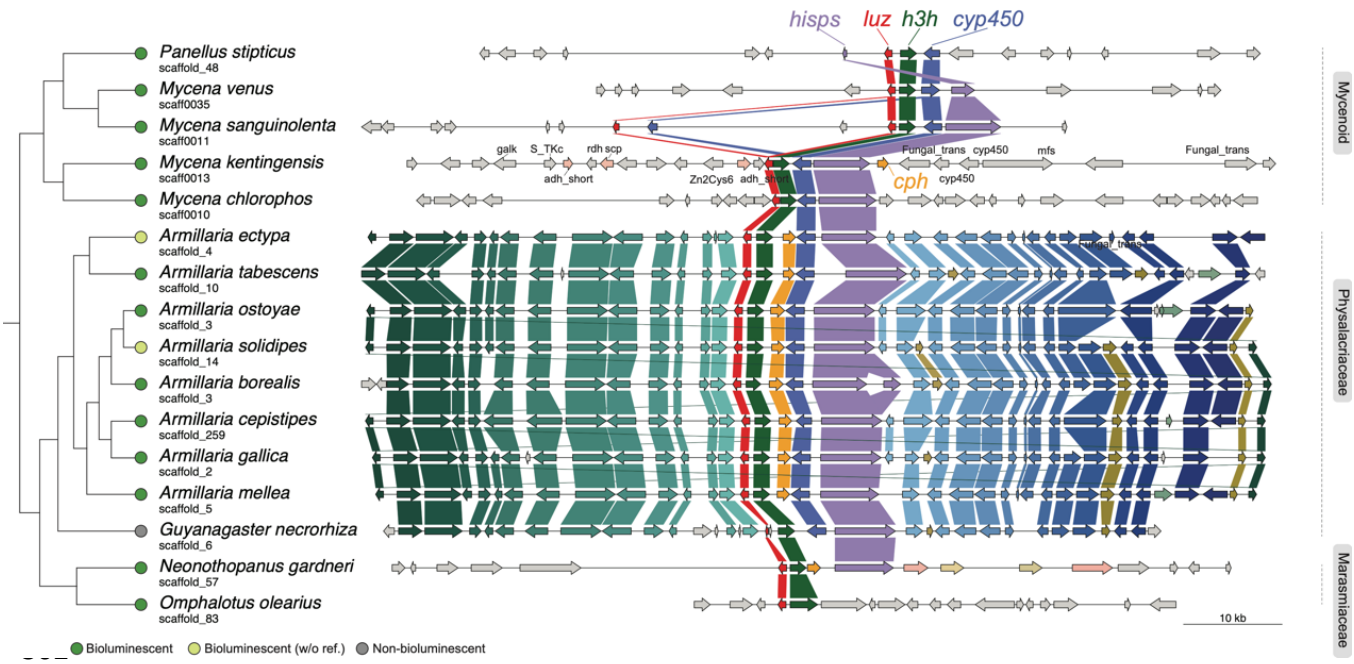

Fig. 4| Synteny around the luciferase cluster among bioluminescent fungi. The orthologous groups (OGs) shared by at least two species were labelled with the same colour, regardless of their orientation. The *cph* gene in some species was located in other scaffolds (Supplementary Fig. 9)

In contrast, the *Mycena* luciferase cluster was identified in the dispensable regions of different linkage groups (**Fig. 3a**), suggesting that the location of the cluster was extensively rearranged since the common ancestor of this lineage. A physical linkage was only maintained in the luciferase cluster, but no synteny was found in adjacent genes (**Fig. 4**). Variations were common amongst the markup of the luciferase cluster. The majority of the *Mycena* luciferase clusters included luciferase (*luz*), hispidin-3-hydroxylase (*h3h*), cytochrome P450 (*cyp450*), and hispidin synthase (*hisps*) (**Fig. 4**). caffeylpyruvate hydrolase (*cph*) was located in different scaffolds in four of the five *Mycena* species (Supplementary Fig. 9). In *M. sanguinolenta*, *luz* and *cyp450* were duplicated adjacent to the luciferase cluster (**Fig. 4**). Losses were observed in different positions of the phylogeny. The non-bioluminescent *M. indigotica* lost the entire luciferase cluster, but an *h3h* homologues were found in other regions of the genome, while *Guyanagaster necrorhiza* has a partial luciferase[6] and three other enzymes (**Fig. 4**), suggesting an independent loss of luciferase function alone was enough for it to lose its bioluminescence. Selection analysis of genes in the luciferase cluster revealed that the majority of conserved sites exhibit either no or strong purifying selection, with only 7–28 sites under episodic selection (Supplementary Fig. 11). Together, these results indicate limited but conserved roles of bioluminescence in the species that have retained

327 bioluminescence.
328
329 These observations lead us to propose a most plausible evolutionary scenario for
330 luciferase cluster evolution across all available bioluminescent fungi genomes (**Fig. 5)**.
331 The earliest ancestral state we could infer was a luciferase cluster having consisted of
332 *luz*, *h3h*, *cyp450*, and *hisps*, with *cph*—involved in oxyluciferin recycling[5,6]—also
333 present in the same chromosome. Such a combination was present in the 14 of the 15
334 bioluminescent species used in this study. The luciferase cluster likely originally
335 formed at the dispensable region. Our model presents two contrasting scenarios by
336 which the luciferase cluster was retained. First, the ancestor of the family
337 Physalacriaceae had its luciferase cluster translocated into the core region. This
338 scenario is based on the uniform observation that all members of *Armillaria* retained
339 the luciferase cluster in their genome, and other members of Physalacriaceae had
340 extended synteny in adjacent genes. The cases of extended synteny, however, were
341 derived from different genomic regions in Agaricales, indicating rearrangements
342 (Supplementary Fig. 10). Second, the luciferase cluster in bioluminescent *Mycena* fungi
343 was conserved, despite being located in a highly rearranged genome partition (**Fig 3a**).
344 Such rearrangements led to higher tendency of loss of luciferase cluster in the mycenoid
345 lineage compared to *Armillaria* species. Additional evidence of rearrangement is that
346 four out of five bioluminescent *Mycena* fungi had at least one gene rearrangement or
347 duplication event compared to their ancestor. Interestingly, we found that *cph* was
348 independently translocated adjacent to the luciferase cluster in both *M. kentingensis* and
349 the ancestor of the marasmioid clade (Supplementary Fig. 12); it was presumably
350 favoured and maintained here by natural selection[39].
351
352 **Fig. 5| Evolutionary scenario for luciferase cluster evolution.** The formation of the luciferase
353 cluster originated at the dispensable region of the last common ancestor and was susceptible to
354 translocate to different genomic locations through rearrangement. In the ancestor of marasmioid,
355 *cph* was duplicated and translocated into the luciferase cluster. Before the ancestor of the
356 Physalacriaceae family emerged, the luciferase cluster was translocated into the core region
357 and have since kept its synteny in the *Armillaria* lineage. In the most recent common ancestor
358 of *Mycena* species, the luciferase cluster was located in the dispensable region and have since
359 been susceptible to further rearrangement. Arrow box indicates gene. The dashed arrow box
360 denotes the loss of gene. Fishhook arrow denotes translocation event. [a] Percentage of
361 bioluminescent fungi found in the mycenoid lineage[40]. [b] Percentage of bioluminescent fungi
362 found in *Armillaria* lineage[41].
363

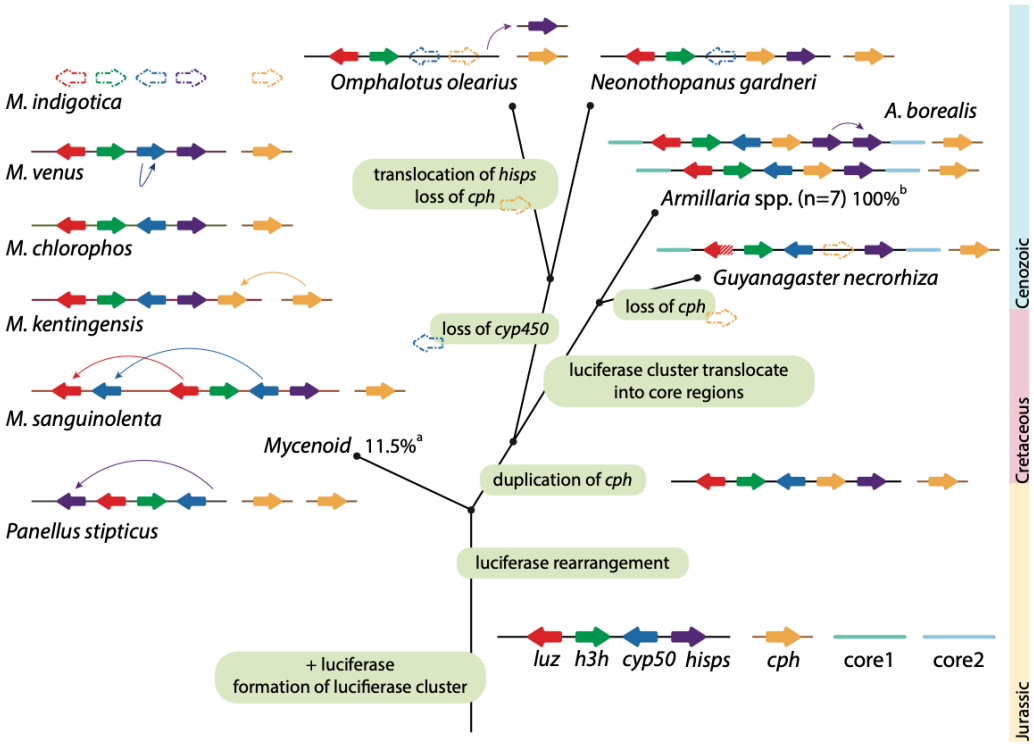

Expression profile of luciferase cluster and identification of conserved genes involved in fungal bioluminescence

Fungal bioluminescence is believed to have ecological roles, such as attracting insects and regulated by circadian rhythms[42]; however, the repertoire of genes involved in bioluminescence are still unknown. We carried out transcriptome profiling between mycelia with different bioluminescent intensities in four *Mycena* species, and identified genes that were either differentially expressed or positively correlated with bioluminescent intensities (Methods). There were 29 OGs found to contain upregulated gene members in all four *Mycena* species (**Fig. 1c and Fig. 6a**), including *luz*, *h3h*, and *hisps,* consistent with that bioluminescence expression depends on the expression of these three genes in the luciferase cluster. In particular, *luz* expression was significantly different between two tissues with relative high and low bioluminescence in *M. kentingensis* (log fold change (logFC) 3.0; adjusted $P< 0.001$) and *M. chlorophos* (logFC 4.7; adjusted $P<0.001$); there was also a significant correlation between bioluminescent intensity and expression level in *M. sanguinolenta* (Pearson's correlation coefficient (PCC) 0.82; $P<0.005$) and *M. venus* (PCC 0.86; $P<0.005$ Supplementary Table 12). In *M. chlorophos*, however, its *cyp450* and *h3h* in the luciferase cluster were not differentially expressed, and four distant homologues of *h3h* were found to be upregulated (Supplementary Fig. 5b). Although a second copy of *luz* and *cyp450* were found in *M. sanguinolenta*, they showed much lower expression (2 and 3 transcripts per million (TPM), respectively) than those in the cluster (282 and 138

387 TPM, respectively). The remaining OGs upregulated in mycelia showing higher
388 bioluminescence included genes involved in ABC transporters and Aceyl-CoA
389 synthetases which also showed a predicted function in metabolic adaptations to
390 bioluminescence in firefly and glowworm[43,44]. (**Fig. 6a**; Supplementary Table 13). In
391 particular, four OGs were annotated as FAD or NAD(P)-binding domain-containing
392 proteins. As these genes do not bear sequence similarity to *h3h* which is also a
393 NAD(P)H-dependent enzyme, they may likely involve in other biochemical processes
394 that is required during bioluminescence.
395
396 Differences in bioluminescent intensity have been recorded in tissues of fungi both in
397 nature[4,40,41,45,46] and—for *M. kentingensis*—in a laboratory environment, in which the
398 life cycle can be completed (**Fig. 6b**). To investigate putative roles of bioluminescence
399 across developmental stages, additional transcriptome profiling was carried out in the
400 primordia, young fruiting body, and cap (pileus) and stipe of the mature fruiting body
401 of *M. kentingensis*. Bioluminescence was stronger in the cap than in the stipe, so we
402 expected the luciferase cluster genes to have higher expression in the cap tissue.
403 However, *luz* and *h3h* showed opposite expression patterns (**Fig. 6c** and Supplementary
404 Table 14), suggesting that there may be other regulators involved in bioluminescence
405 in *M. kentingensis*.
406
407 The regulation of bioluminescence in *M. kentingensis* during development was
408 determined by performing a weighted correlation network analysis (WGCNA[47,48]),
409 which identified 67 modules of co-expressed genes in these stages (Supplementary Fig.
410 14). All members of the luciferase cluster *luz*, *h3h*, *cyp450*, and *hisps* belonged to the
411 same module (Module50; **Fig. 6c**) of 57 genes, suggesting that the expression of the
412 luciferase cluster members are orchestrated during developmental stages. Only two
413 genes belonging to OG0001818 (acid protease) and OG0000000 (short-chain
414 dehydrogenase) which were part of the 29 aforementioned OGs involved in
415 bioluminescence of the mycelium across *Mycena*. Six genes in this module were
416 annotated as carbohydrate-active enzymes (Supplementary Table 15): one GH75
417 (chitosanase), one AA1_2 (Laccase; ferroxidases), two GH16, and two genes with two
418 CBM52. GH16 (glucanases) and AA1 (laccases) are known to be regulated during
419 fruiting body development[49], implying a possible link between cell wall remodelling
420 during development and bioluminescence. In addition, we re-analysed the
421 transcriptomes of *Armillaria ostoyae* across different developmental stages from Sipos
422 *et al*. (2017)[8]. Consistent with observation that bioluminescence was only observed in
423 mycelia and rhizomorphs in *A. ostoyae*[50,51], the expression of *luz*, *h3h*, *cyp450*, and *cph*
424 showed highest expression before the primordia stage (Supplementary Fig. 15).

Together, these results imply that luciferase cluster was differentially regulated during developmental stages; extent of regulation were also different in bioluminescent species of different lineages.

Fig. 6| Expression analysis to identify genes involved in bioluminescence. a, Conserved upregulated OGs. Differentially-expressed genes (DEGs) between mycelia with different bioluminescent intensities were identified in four bioluminescent *Mycena* species, and all 29 OGs—except OG0009249 and OG0000706—contain at least one upregulated gene. A detailed annotation of the genes in the OGs is listed in Supplementary Table 13. The raw gene number in each OG is shown in Supplementary Fig. 13. **b**, Tissues used for transcriptomic data analysis in *M. kentingensis*. The left and right side are the tissues under light and dark conditions, respectively (captured by a Nikon D7000). The camera setting for each tissue: mycelium, Sigma 17-50mm ISO100 f2.8 with 16 min exposure time; primordia, AF-S Micro Nikkor 60mm ISO800 f/11with 122.4 sec exposure time; YFB, AF-S Micro Nikkor 60mm ISO800 f/11with 60.6 sec exposure time; FB, AF-S Micro Nikkor 60mm ISO800, f/11 with 9.3 sec exposure time. YFB, young fruiting body (0.5-1 cm). FB, mature fruiting body (> 1 cm). FB-cap, cap from FB. FB-stipe, stipe from FB. **c**, Expression profile of luciferase cluster across developmental stages of *M. kentingensis*. Bold lines indicate four genes in the luciferase cluster. These four genes and the other 53 genes (yellow) were assigned into the same module (Module50) with similar expression patterns. The genes located up- or downstream (grey) of the luciferin biosynthesis cluster had lower expression levels than the four genes in the cluster.

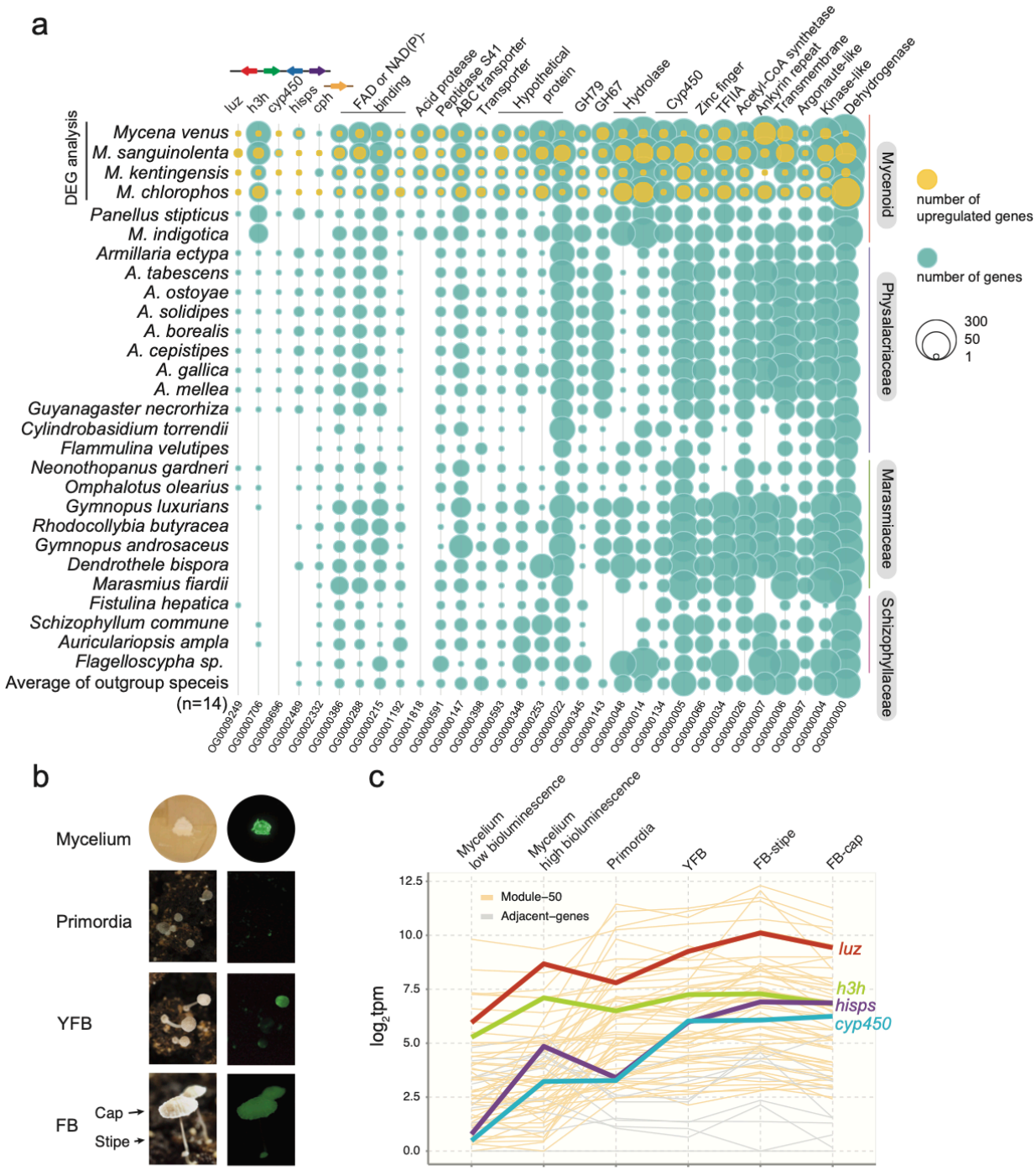

Gene families associated with the evolution of mycenoid species

We sought to identify proteins specific to mycenoid species by annotating protein family (Pfam) domains and comparing them with those of species outside this lineage (Supplementary Table 16). A total of 537 Pfam domains were enriched in the mycenoid lineage (one-fold by Wilcoxon rank sum test with $P<0.01$; Supplementary Table 17) of

which 3–17 were species-specific. Acyl_transf_3 (acyltransferase family; PF01757), contained in a range of acyltransferase enzymes, was the only domain found in all six mycenoid species. The closest homologs were found in ascomycetous *Cadophora*, *Pseudogymnoascus*, or *Phialocephala* (31-35% identity with 73-100% coverage). Four of the enriched domains are known pathogenesis-related domains expanded in pathogenic Agaricales *Moniliophthora*[52] and *Armillaria* species[8]: COesterase (PF00135; Carboxylesterase family), Thaumatin (PF00314), NPP1 (PF05630; necrosis-inducing protein), and RTA1 (PF04479; RTA1-like protein) (Supplementary Fig. 16). Moreover, *M. sanguinolenta* and *M. venus* contained over 100 and 17 copies of COesterase and Thaumatin (median 37 and 4 copies in other fungal species of this study), respectively.

Wood decay gene repertoires in *Mycena* species

Since studies on wood degradation in *Mycena* are lacking[53], we annotated the carbohydrate-active enzyme (CAZyme) repertoire of *Mycena* proteomes to understand their ecological role. Class II peroxidases (AA2) were identified in all *Mycena* species, suggesting these species can degrade lignin and leave white coloured cellulose (white rot) behind[54]. In particular, *M. sanguinolenta* and *M. venus* possess 66 and 72 copies of AA2, respectively, which are much higher than in other closely-related white-rot fungi, such as *Armillaria* species (10–14 copies). *Mycena* species also contain 11–20 copies of AA5_1 (copper radical oxidases), 18–121 copies of AA3_2 (GMC oxidoreductase), and 10–34 copies of AA1_1 (Laccases)[55]. These enzymes are capable of degrading or modifying lignin and are generally in higher abundance in white-rot than in brown-rot fungi[55,56]. For cellulose degradation, white-rot generally has more cellulolytic genes—i.e., GH6 and GH7—and lytic polysaccharide monooxygenase of AA9 than does brown-rot fungi[55]. Our *Mycena* species have similar numbers of these genes as other white-rot fungi (Supplementary Fig. 17).

Discussion

Bioluminescence is one of the most unusual and fascinating traits in fungi, but the evolutionary history of luciferase cluster remains elusive. Here, we produced highly contiguous genome assemblies using Nanopore technology and annotations for five of the *Mycena* species to examine their genome dynamics. The results of phylogenomic analyses on these genomes have important implications for the origin of luciferase. We argue that luciferase originated in the last common ancestor of mycenoid and marasmioid, which disagrees the theory of Kotlobay *et al.*[6], that it originated at the basal clade of Agaricales. Our results are in good general agreement with comparative

genomic analyses around this group[8], and is the more evolutionarily parsimonious scenario that does not require an extensive loss of luciferase across the entire Agaricales lineage (**Fig. 1b** and **1c**).

Until 2019, only 68 species of bioluminescent fungi were known[40] across over 600 non-bioluminescent ones in Mycenaceae. Our reconstructed evolution of the luciferase cluster model shows that the luciferase cluster originated in the dispensable region of genomes (**Fig. 3**), making it susceptible to rearrangement, which suggests it is highly prone to loss and explains why most mycenoid species are non-bioluminescent. This is consistent with a previous report that the main evolutionary process in fungal gene clusters is vertical evolution followed by differential loss[57]. Interestingly, synteny was retained in luciferase clusters and adjacent genes of *Armillaria* species (**Fig. 4**), which are better known for their roles as plant pathogens[8]. Indeed, bioluminescence was identified in all nine examined *Armillaria* species[41]. We speculate that the majority of unquantified *Armillaria* species may also exhibit bioluminescence. The repeated duplication and relocation of *cph* that we observed in the luciferase cluster is under selection pressure, suggesting that bioluminescence has adaptive importance in these species. A systematic quantification of bioluminescence and more complete genome assemblies will help reconstruct the evolutionary events that contributed to the polymorphism and functional diversity in the luciferase clusters.

Chromosome-length polymorphisms are uncommon in Agaricales but have been observed in the pathogen *Moniliophthora perniciosa*[58] causing witches' broom disease and model mushroom *Coprinopsis cinerea*[59]. Synteny analyses across *Mycena* genomes revealed the first documented case of 'two speed' genomes in the Agaricales. Despite all the studied *Mycena* species are saprotrophs, the compartmentalization of genomes exhibiting contrasting evolutionary scenarios and the presence of lineage-specific chromosomes are hallmarks of plant pathogens throughout fungal tree of life[60]. We argue that in addition to gene family expansion and adaptation due to diversifying lifestyle, the increased rates of evolution in particular regions have also led to higher propensity to the loss of luciferase cluster in the mycenoid lineage. Two of the five *Mycena* species had large genomes, which was a result of a transposable element expansion and gene family dynamics (**Fig. 1d**). In plants, animals and fungi, DNA methylation is known to suppress TE activity[61,62]. In *Mycena*, we observed numerous relic TEs containing sequences similar to classic TEs but lacking functional domains, and these relic TEs had lower levels of CG methylation than did the classic TEs (**Fig. 2b**). We hypothesize that the relic TEs were still repressed by DNA methylation, yielding overall lower levels of CG methylation in active TEs, which consequently

533 resulted in genome expansion and increased dispensable region offering more plasticity
534 in their evolution.
535
536 Researchers have long been puzzled over the ecological role of bioluminescence in
537 fungi. One explanation that has been put forth for *Neonothopanus gardneri* is that
538 bioluminescence follows a circadian rhythm to increases spore dispersal by attracting
539 arthropods in the evening[42]. If true, this is most likely a derived adaptation, as most
540 Agaricomycetes like *Omphalotus nidiformis* disperse spores via wind, display
541 bioluminescence continuously, and do not attract insects[63]. Besides, attraction is
542 insufficient to explain luminescence in the mycelium. *Mycena kentingensis* and
543 *Armillaria ostoyae* are thought to constitutively express the luciferase cluster
544 throughout development[64]. In addition to the luciferase cluster, only a handful of genes
545 were identified to associate with fungal bioluminescence (**Fig6**). If fungal
546 bioluminescence originated as a by-product of a biological process that is currently
547 unknown, the ecological role was likely to be initially limited and has undergone
548 subsequent losses in many species, especially in the *Mycena* lineage. For those that
549 have retained bioluminescence, we speculate that its ecological role may be species-
550 specific and together converge on the maintenance of luciferase cluster.
551
552 In summary, our comparative analyses have led us to propose an evolutionary model
553 pinpointing changes in the luciferase cluster across all published bioluminescent
554 species. Our findings offer insights into the evolution of a gene cluster spanning over
555 160 million years and the retained luciferases were under strong purifying selection.
556 Our *Mycena* genome sequences may complement ongoing research on the application
557 of bioluminescent pathways[6] and shed light on the ecological role of bioluminescence
558 in fungi.
559

560 # Methods

561

562 **Strains and fungal materials**

563 *M. kentingensis*, *M. venus, M. sanguinolenta, M. indigotica* and *M. chlorophos* were
564 isolated from fruiting bodies collected from forest in Taiwan. *M. indigotica* was
565 isolated from basidiospores. The mycelia were grown and maintained on potato
566 dextrose agar (PDA) plates at 25°C. To identify the pattern of bioluminescence, a
567 piece of mycelium from each species was inoculated in the centre of a sheet of
568 sterilized dialysis cellulose membrane (8030-32, Cellu Sep T-Series) on a 3 cm PDA
569 agar plate at 25°C. The diameter of the mycelium was measured and its

570 bioluminescence was recorded with a Glomax 20/20 luminometer (Promega
571 BioSystems Sunnyvale, Inc., USA) for seven days (Supplementary Table18). The
572 taxonomic status of species was reconfirmed by sequencing the internal transcribed
573 spacer (ITS) with the primer pair SR6R(5'-AAGWAAAAGTCGTAACAAGG-
574 3')/ITS4(5'-TCCTCCGCTTATTGATATGC-3'). Using the other available *Mycena*
575 ITS sequences, all sequences were aligned by MAFFT[65] (ver. 7.310) and trimmed by
576 trimAl[66] (1.2rev59; with option -automated1). The ITS phylogeny was constructed by
577 IQ-TREE[67,68] (ver. 1.6.10; with option -bb 10000 -alrt 1000).
578
579 **Genomic DNA extraction and sequencing**
580 Genomic DNA was extracted using the traditional CTAB and chloroform extraction
581 method. Briefly, 0.1 g mycelium was grinded with liquid nitrogen and then mixed with
582 CTAB extraction buffer (0.1 M tris, 0.7 M NaCl, 10 mM EDTA, 1% CTAB, 1% Beta-
583 Mercaptoethanol). After incubating at 65°C for 30 min, an equal volume of chloroform
584 was added, then the mixture was centrifuged at 8000 rcf for 10 min. The supernatant
585 was mixed with an equal volume of isopropanol and the DNA was precipitated. After
586 washing with 70% EtOH, the DNA was dissolved with nuclease free water. Genome
587 sequencing was carried out in two platforms. First, paired-end libraries were
588 constructed using the KAPA LTP library preparation kits (#KK8232, KAPA
589 Biosystems). All libraries were prepared in the High Throughput Genomics Core at
590 Biodiversity Research Center, Academia Sinica and sequenced on an Illumina HiSeq
591 2500 platform. A total of 51.6 Gb of 150- or 300-bp read pairs were generated. Second,
592 Oxford Nanopore libraries were prepared using SQK-LSK108 and sequenced on a
593 GridION instrument. Basecalling of Nanopore raw signals was performed using Guppy
594 (ver. 3.2.4) into a total 67.7 Gb of raw sequences at least 1 kb or longer. A summary of
595 the sequencing data is shown in Supplementary Table 1.
596
597 **RNA extraction and sequencing**
598 Bioluminescent mycelia were collected in two ways. i) For *M. chlorophos* and *M.*
599 *kentingensis*, a piece of mycelium was inoculated at the centre of a sheet of sterilized
600 dialysis cellulose membrane (8030-32, Cellu Sep T-Series) on PDA agar plates at 25°C.
601 The plates were cultured for 10 and 14–18 days for *M. chlorophos* and *M. kentingensis*,
602 respectively. For *M. kentingensis*, bioluminescence was detected by camera (Nikon
603 D7000, Sigma 17-50mm ISO100 f2.8 with 16 min exposure time) (**Fig. 6b**). The
604 mycelia with low or high bioluminescent intensities which occurred spontaneously
605 were collected from two separated plates inoculated on the same day. In *M. chlorophos*,
606 bioluminescence was detected by luminometer. Mycelium with low bioluminescence
607 showed the intensity of 7-14 Relative Light Unit (RLU)/mg, and the mycelium with

608 high bioluminescence showed the intensity of 5,000-10,000 RLU/mg (Supplementary
609 Table 3). Three replicates were collected. ii) For *M. sanguinolenta* and *M. venus*, a piece
610 of mycelium was inoculated at the centre of a sheet of sterilized dialysis cellulose
611 membrane on PDA agar plates at 25°C. The plates were cultured for 13–17 days, and
612 the bioluminescent features were detected by CCD camera; the tissues were collected
613 and their luminescence intensity was recorded with a Glomax 20/20 luminometer
614 (Promega BioSystems Sunnyvale, Inc., USA). A total of 12 samples with different
615 bioluminescence intensities were collected (Supplementary Table 3). After
616 homogenizing 5–10 mg of tissues by liquid nitrogen, total RNA was extracted using
617 the Direct-zol RNA Miniprep (Zymo Research). Concentrations were measured by
618 Qubit fluorometer (Invitrogen USA), and quality was assessed by the BioAnalyzer
619 2100 RNA Nano kit (Agilent, USA) with RIN values higher than 8.0. The paired-end
620 libraries were constructed using the TruSeq Stranded mRNA library prep kit
621 (#20020594, Illumina, San Diego, USA) with standard protocol and sequenced by
622 Illumina HiSeq 2500 (Illumina, USA) to produce 150-bp paired-end reads.
623
624 **RNA extraction and sequencing from the *M. kentingensis* fruiting body**
625 Fruiting body production of *M. kentingensis* was modified from previous studies[69,70].
626 Mycelia, grown on PDA for 8–15 days, was then inoculated onto sterilized
627 commercially available peat soil mixed with 10% rice bran and 50% water in a jar.
628 Mycelium samples were grown at 25°C for 3–4 weeks and then transferred into fresh
629 compost. The culture was sprayed with sterilized water daily until the fruiting body
630 formed. Four kinds of tissue were collected: (1) primordia, (2) young fruiting body
631 (YFB, 0.5–1 cm), (3) cap and (4) stipe of mature fruiting body (> 1 cm). For each batch
632 of culture, 15–20 primordia, 6–11 YFB, and 8–12 caps and stipes from mature fruiting
633 bodies were pooled to measure their weight and bioluminescent intensity, and the RNA
634 was extracted using Trizol extraction and lithium chloride purification method. Three
635 replicates were produced. The paired-end libraries were constructed using the TruSeq
636 Stranded mRNA library prep kit (#20020594, Illumina, San Diego, USA) with standard
637 protocol and sequenced by Illumina HiSeq 2500 (Illumina, USA) to produce 150-bp
638 paired-end reads.
639
640 ***De novo* assemblies of *Mycena* species**
641 Oxford Nanopore reads were assembled using the Canu[71] (ver. 1.8) assembler.
642 Consensus sequences of the assemblies were polished first by five iterations of Racon[72]
643 (ver. 1.3.2) followed by Medaka (ver. 0.7.1; https://github.com/nanoporetech/medaka)
644 using Oxford Nanopore reads. HaploMerger2[73] (ver. 20180603) was then run on to
645 generate haploid assemblies. Finally, the consensus sequences were further corrected

646 with Illumina reads using Pilon[74] (ver. 1.22). Throughout each stage the genome
647 completeness was assessed using fungi and basidiomycete dataset of BUSCO[15] (ver.
648 3.0.2). Putative telomeric repeats were searched for copy number repeats less than 10
649 mers using tandem repeat finder[75] (ver. 4.09; options: 2 7 7 80 10 50 500). The hexamer
650 TTAGGG was identified (Supplementary Table 19).
651
652 **Gene predictions and functional annotation**
653
654 Protein sequences from Uniprot fungi (32,991 sequences; downloaded 20th December
655 2018) and *Coprinopsis cinerea, Pleurotus ostreatus* PC15 (v2.0), *Schizophyllum*
656 *commune and Armillaria mellea* from MycoCosm[76] portal were downloaded as
657 reference proteome. Transcriptome reads were first mapped to the corresponding
658 genome assemblies using STAR[77,78] (ver. 2.5.3a), and subsequently assembled into
659 transcripts using Trinity[79] (ver. 2.3.2; guided approach), Stringtie[80] (ver. 1.3.1c),
660 CLASS2[81] (ver. 2.1.7) and Cufflinks[82] (ver. 2.2.1). The samples used for input are listed
661 in Supplementary Table 3. Transcripts generated from Trinity were aligned to the
662 references using GMAP[83]. All transcripts were merged, filtered and picked using
663 MIKADO[84] (ver. 1.1). The gene predictor Augustus[85] (ver. 3.2.1) and gmhmm[86] (ver.
664 3.56) were trained using BRAKER2[87] (option fungi and softmasked), and SNAP[88] was
665 trained using the assembled transcripts with MAKER2[14] (ver. 2.31.9). The assembled
666 transcripts, reference proteomes and BRAKER2 annotations were combined as
667 evidence hints for input in the MAKER2[14] annotation pipeline. MAKER2[14] invoked
668 the three trained gene predictors to generate a final set of gene annotation. Amino acid
669 sequences of the proteome were functionally annotated using Blast2GO[89] and eggnog-
670 mapper[90] (ver. 1.0.3).
671
672 **Identification of repetitive elements**
673 Consensus (library) sequences of repetitive elements were identified using the
674 pipeline described in Berriman *et al*[91]. Full LTR retrotransposons in *Mycena* species
675 were defined as i) initially identified by LTRharvest[92] and ii) presence of known
676 reverse transcriptase domains identified by Pfam[93] (ver. 31.0). Repeat contents were
677 quantified using RepeatMasker[94] (ver. open-4.0.7). Proportions of repeat content
678 along the scaffolds were calculated using Bedtools[95]. A phylogenetic tree was built by
679 first aligning all the putative RVT domain sequences using MAFFT[65] (ver. 7.310; --
680 genafpair --ep 0) and FastTree[96] with the JTT model on the aligned sequences, and
681 were visualised using the ggtree[97] package in R.
682
683 **Methylation analyses**

684 To construct a BS-seq library, the fragmented DNA was first ligated with a
685 premethylated TruSeq DNA adapter (Illumina). The ligated DNA fragments were
686 bisulfite converted using the EZ DNA methylation kit (Zymo Research), followed by
687 PCR amplification. The BS-seq libraries were sequenced on an Illumina HiSeq 2500
688 sequencer. The bisulfite conversion efficiency reached approximately 99% in all of our
689 libraries (Supplementary Table 20). High-quality paired-end reads were aligned to the
690 genome assemblies of *M. kentingensis* using the bisulfite specific aligner BS-Seeker2[98].
691 Only uniquely mapped reads were retained. The cytosines covered by at least four reads
692 were included in the data analysis, and the DNA methylation level for each cytosine
693 was estimated as #C/(#C+#T), where #C is the number of methylated reads and #T is
694 the number of unmethylated reads.
695
696 One or two Nanopore flowcells for each Mycena species were selected to infer
697 methylation information using deepsignal[99] (ver. 0.1.5) (*M. kentingensis*: FAH31207,
698 *M. chlorophos*: FAH31470, *M. indigotica*: FAH31228, *M. sanguinolenta*: FAK22405
699 and FAH31211, *M. venus*: FAK22389 and FAH31302). The machine learning-based
700 model was trained with one bisulfite dataset (YJMC0389) and one Nanopore dataset
701 (FAH31207) of *M. kentingensis*. The bisulfite result was first filtered for depth >20,
702 then methylation levels >0.9 and <0.01 were selected for positive and negative
703 validation datasets, respectively. All seven flowcells were called for methylation
704 information with a customized model and default arguments. A minimal depth of 4 was
705 applied to the results for further analysis. In the estimates of DNA methylation levels
706 between Nanopore long-reads and the Illumina BS-seqs, the Pearson correlation
707 coefficient was as high as 0.96 in the methylomes of *M. kentingensis* (Supplementary
708 Fig. 18).
709
710
711 **Orthogroup inference and analysis of protein family domains**
712 Orthologous groups (OGs) among 42 species were identified using OrthoFinder[16,17]
713 (ver. 2.2.7). CAFÉ[18] (ver. 4.2.1) was used to predict the expansion and contraction of
714 gene numbers of OGs based on the topological gene tree. Unique OGs among the
715 node identified by CAFÉ were analysed by UpSetR[100]. The phylogenetic tree was
716 visualized by the ggtree[97,101] package in R. Protein domains of each gene were
717 identified by pfam_scan.pl ver. 1.6 by comparing them against Pfam ver. 32.0 db[93]. To
718 compare them to plant pathogenic fungi, the Pfam domains from *Moniliophthora*
719 *perniciosa* FA55313 (Monpe1_1)[52] from JGI and *Moniliophthora roreri* (Monro)
720 from BioProject: PRJNA279170 were also annotated. Enrichment of Pfam domain
721 number between two sets of interest was assessed by the Wilcoxon rank-sum test ($P \leq$

722 0.05). We compared the Pfam copy number between six mycenoid species and the
723 other 37 species. Gene ontology enrichments were identified for these genes using
724 TopGO[102]. Genes encoding carbohydrate-active enzymes were identified according to
725 the Carbohydrate-Active enZYmes (CAZy) Database[103] by searching for sequence
726 homologs with DIAMOND[104] or HMMER[105].
727
728 **Phylogenomic analyses**
729 A total of 42 sets of amino acid sequences from 360 single-copy OGs were aligned
730 independently using MAFFT[65] (ver. 7.271; option --maxiterate 1000). A total of three
731 approaches were used to infer the species tree. The first two approaches relied on
732 maximum likelihood phylogenies from individual OG alignments computed using
733 RAxML-ng[106] (ver. 0.9.0; options: --all --model LG+I+F+G4 --seed 1234 --tree pars 10
734 --bs-trees 100) with 100 bootstrap replicates. The best phylogeny and bootstrap
735 replicates were separately used to infer a consensus tree using ASTRAL-III[20]. Finally,
736 a maximum likelihood phylogeny from the concatenated amino acid alignments of the
737 single-copy orthogroups was constructed with 100 bootstrap replicates using RAxML-
738 ng[106] (ver. 0.9.0; options: --all --seed 1234 --tree pars 10 --bs-trees 100 with --model
739 LG+I+F+G4 partitioned with each OG alignment).
740
741 **Estimation of divergence time**
742 The divergence time of each tree node was inferred using MCMCtree in PAML[21]
743 package (ver. 4.9g with approximate likelihood[107]; the JC69 model and the rest were
744 default). The species tree and concatenated translated nucleotide alignments of 360
745 single-copy-orthologs were used as the input for MCMCtree. The phylogeny was
746 calibrated using fossil records by placing soft minimum bounds at the ancestral node
747 of: i) marasmioid (using *Archaeomarasmius legettii* 94–90 Ma[108]; 90 was used), ii)
748 Agaricales (using *Palaeoagaricites antiquus* 110–100 Ma[109]; 100 was used), iii) Taxon
749 A (~99 Ma[110]; 95 was used), and iv) a soft bound of 200 Ma for the phylogeny. The
750 entire analysis was run five times to check for convergence.
751
752
753 **Synteny analyses**
754 Linkage groups (LGs) between *M. indigotica* and *Armillaria ectypa,* and between *M.*
755 *indigotica* and *Pleurotus ostreatus* were assigned based on the majority of the single-
756 copy orthologues (Supplementary Figure 7 and 8). Scaffolds containing fewer than 10
757 single-copy orthologues, shorter than 500 kb or species N90 were excluded. Linkage
758 groups within *Mycena* were assigned based on majority and at least 10% of single-copy
759 orthologue links with *M. indigotica* scaffolds. Subsequent scaffolds were identified as

760 the same linkage group if they contained a majority of pairwise one-to-one single-copy
761 orthologues belonging to the *M. indigotica* LG.
762
763 As gene collinearity among *Mycena* species became less conserved, synteny blocks of
764 each *Mycena* species were defined based on merging of adjacent pairwise single-copy
765 orthologues to its closest-related species. For instance, synteny blocks of *M. chlorophos*
766 were based on single-copy orthologues against *M. indigotica*. For every ortholog, the
767 distance to the next closest single-copy orthologue was calculated to take into account
768 segment duplications of genes or gene insertion/deletions. Synteny blocks within the
769 90% quantile of ortholog distance were further merged and classified as core regions.
770 Dispensable regions were defined as synteny breaks under this criterion. Based on these
771 criteria, 68.5–85.5% of the genomes of *Mycena* species were dispensable
772 (Supplementary Table 21). Synteny around luciferase cluster was based on orthogroup
773 sharing and plotted using the R genoPlotR[111] package.
774
775
776 **Evolution of gene families related to the luciferase gene cluster**
777 The sequences of five orthologues in the luciferase family—hispidin-3-hydroxylase,
778 cytochrome P450, hispidin synthase, and caffeylpyruvate hydrolase—were
779 constructed and the sequences were aligned by MAFFT[65] (ver. 7.310) and trimmed by
780 trimAl[66] (1.2rev59 ; with option -automated1). The protein trees were constructed by
781 IQ-TREE [67,68] (ver. 1.6.10; with option -bb 10000 -alrt 1000). The evidence for
782 selection across gene families was tested using the HyPhy[112,113] platform in the
783 webserver of datamonkey[114-116]. According to the recombination breakpoints analysed
784 by the Genetic Algorithm for Recombination Detection[117] (GARD), the alignment
785 was trimmed for analysing selection using Single-Likelihood Ancestor Counting[118]
786 (SLAC) and Mixed Effects Model of Evolution[119] (MEME) with $P<0.1$.
787
788
789 **RNAseq analysis of differential bioluminescent mycelium**
790 Quality trimming of the RNA sequencing reads was conducted using Trimmomatic[120].
791 The sequencing reads were mapped to the genome using STAR[77,78] (ver.
792 STAR_2.5.1b_modified; default parameters). Raw read counts of the gene models were
793 quantified by FeatureCounts[121] (ver. v1.5.0; -p -s 2 -t exon). For *M. kentingensis* and *M.*
794 *chlorophos*, the differential expressed genes (DEGs) were analysed using DESeq2[122].
795 Genes with fold change (FC) > 0 and FDR ≤ 0.05 were defined as DEG. *For M.*
796 *sanguinolenta* and *M. venus*, the DEGs were identified by the Pearson correlation
797 coefficient between the bioluminescence intensity (relative light unit; RLU) normalized

by weight (RLU/mg) and log transformation of counts per million. Genes with correlation coefficient > 0.7 and $P<0.01$ were defined as DEGs.

RNA analysis of *M. kentingensis* and *Armillaria ostoyae* developmental stages

The reads from transcriptomes of the primordia, young fruiting body, and cap and stipe of mature fruiting body were conducted by the same method of manipulating the reads from transcriptomes of mycelium. To identify co-expressed genes among transcriptomes, the transformation of transcripts per million (TPM) from six different tissues—mycelia with high bioluminescence and low bioluminescence, primordia, young fruiting body, and fruiting body cap and stipe were calculated. The lowest 25% expressed gene across all samples were excluded and co expression was analysed using weighted gene co-expression network analysis (WGCNA)[47,48] package in R (maxBlockSize = 10000, power = 20, networkType = signed , TOMType = signed, minModuleSize = 30). The Illumina reads among ten stages from *Armillaria ostoyae* were also downloaded from NCBI's GEO Archive (http://www.ncbi.nlm.nih.gov/geo under accession GSE100213) and also analysed by the same pipeline of *M. kentingensis* to identify co-expressed genes among the transcriptomes.

Authors contribution

I.J.T. and H.M.K. conceived the study. I.J.T. led the study. H.M.K., C.C.C., G.S. and H.W.K. collected and identified *Mycena* species around Taiwan. H.M.K, P.H.W. and C.I.L. conducted the experiments. M.J.L. and J.Y.L. designed the illumina sequencing experiment. H.H.L. and I.J.T. performed the assemblies and annotations of the *Mycena* genomes. H.M.K., H.H.L., Y.C.L. and I.J.T. conducted the repeat analysis. L.C.N. and I.J.T. carried out phylogenomics analyses and the divergence time estimation. H.M.K., H.H.L., Y.C.L. and I.J.T. carried out comparative genomic analyses. H.M.K. and M.R.L. analysed the RNA-seq data. H.H.L., R.J.L., J.W.H., P.Y.C. and H.M.K. carried out the methylation analyses. H.M.K. and I.J.T. wrote the manuscript with input from L.C.N and P.Y.C.

Acknowledgement

We thank Chia-Ning Shen for lending us the luminometer for the duration of the project. We thank Bi-Chang Chen for providing the CCD camera to qualify bioluminescence. We thank Chi-Yu Chen and Jie-Hao Ou for their useful advice on culturing *Mycena* fungi. We are grateful to the '1000 Fungal Genomes – Deep Sequencing of Ecologically-relevant Dikarya' consortium for access to unpublished genome data. We thank Gregory Bonito, Hui-Ling Liao, Alejandro Rojas and Rytas Vilgalys for permission to use the *Flagelloscypha* sp. FlaPMI526_1 assembly from JGI. We thank Mary Catherine Aime for permission to use the *G. necrorhiza* MCA 3950. assembly from JGI. The genome sequence data were produced by the US Department of Energy Joint Genome Institute (JGI) in collaboration with the user community. We thank Chia-Lin Chung, Ben-Yang Liao and John Wang for commenting the earlier version of the manuscript. P.Y.C was supported by Ministry of Science and Technology, Taiwan, under Grant No. 106-2311-B-001 -035 -MY3 and 108-2313-B-001 -013 -MY3. H.M.K was supported by postdoctoral fellowship, Academia Sinica. I.J.T was supported by Career Development Award AS-CDA-107-L01, Academia Sinica.

Data availability

Genome assembly and annotation of five *Mycena* species was deposited in the National Centre for Biotechnology Information BioProject database (accession no. PRJNA623720) pending final checks.

References

1 He, M. *et al.* Notes, outline and divergence times of Basidiomycota. *Fungal Diversity*, doi:10.1007/s13225-019-00435-4 (2019).

2 Wei, C. & Kirschner, R. A new Mycena species with blue basidiomata and porioid hymenophore from Taiwan. *Mycoscience* **60**, 10-13, doi:10.1016/j.myc.2018.06.001 (2019).

3 Thoen, E. *et al.* In vitro evidence of root colonization suggests ecological versatility in the genus Mycena. *New Phytologist*, doi:10.1111/nph.16545 (2020).

4 Chew, A., Desjardin, D., Tan, Y., Musa, M. & Sabaratnam, V. Bioluminescent fungi from Peninsular Malaysia-a taxonomic and phylogenetic overview.

874 *Fungal Diversity* **70**, 149-187, doi:10.1007/s13225-014-0302-9 (2015).
875 5 Kaskova, Z. M. *et al.* Mechanism and color modulation of fungal
876 bioluminescence. *Sci Adv* **3**, e1602847, doi:10.1126/sciadv.1602847 (2017).
877 6 Kotlobay, A. A. *et al.* Genetically encodable bioluminescent system from fungi.
878 *Proc Natl Acad Sci U S A* **115**, 12728-12732, doi:10.1073/pnas.1803615115
879 (2018).
880 7 Varga, T. *et al.* Megaphylogeny resolves global patterns of mushroom evolution.
881 *Nat Ecol Evol* **3**, 668-678, doi:10.1038/s41559-019-0834-1 (2019).
882 8 Sipos, G. *et al.* Genome expansion and lineage-specific genetic innovations in
883 the forest pathogenic fungi Armillaria. *Nat Ecol Evol* **1**, 1931-1941,
884 doi:10.1038/s41559-017-0347-8 (2017).
885 9 Floudas, D. *et al.* Evolution of novel wood decay mechanisms in Agaricales
886 revealed by the genome sequences of Fistulina hepatica and Cylindrobasidium
887 torrendii. *Fungal Genet Biol* **76**, 78-92, doi:10.1016/j.fgb.2015.02.002 (2015).
888 10 Park, Y. J. *et al.* Whole genome and global gene expression analyses of the
889 model mushroom Flammulina velutipes reveal a high capacity for
890 lignocellulose degradation. *PloS one* **9**, e93560,
891 doi:10.1371/journal.pone.0093560 (2014).
892 11 Liu, D., Hunt, M. & Tsai, I. J. Inferring synteny between genome assemblies: a
893 systematic evaluation. *Bmc Bioinformatics* **19**, 26, doi:10.1186/s12859-018-
894 2026-4 (2018).
895 12 Heinzelmann, R., Rigling, D., Sipos, G., Münsterkötter, M. & Croll, D.
896 Chromosomal assembly and analyses of genome-wide recombination rates in
897 the forest pathogenic fungus Armillaria ostoyae. *Heredity*, doi:10.1038/s41437-
898 020-0306-z (2020).
899 13 Perez, G., Pangilinan, J., Pisabarro, A. G. & Ramirez, L. Telomere organization
900 in the ligninolytic basidiomycete Pleurotus ostreatus. *Appl Environ Microbiol*
901 **75**, 1427-1436, doi:10.1128/AEM.01889-08 (2009).
902 14 Holt, C. & Yandell, M. MAKER2: an annotation pipeline and genome-database
903 management tool for second-generation genome projects. *BMC bioinformatics*
904 **12**, 491, doi:10.1186/1471-2105-12-491 (2011).
905 15 Simão, F. A., Waterhouse, R. M., Ioannidis, P., Kriventseva, E. V. & Zdobnov,
906 E. M. BUSCO: assessing genome assembly and annotation completeness with
907 single-copy orthologs. *Bioinformatics* **31**, 3210-3212,
908 doi:10.1093/bioinformatics/btv351 (2015).
909 16 Emms, D. M. & Kelly, S. OrthoFinder: phylogenetic orthology inference for
910 comparative genomics. *Genome Biol* **20**, 238, doi:10.1186/s13059-019-1832-y
911 (2019).

17 Emms, D. M. & Kelly, S. OrthoFinder: solving fundamental biases in whole genome comparisons dramatically improves orthogroup inference accuracy. *Genome Biol* **16**, 157, doi:10.1186/s13059-015-0721-2 (2015).

18 De Bie, T., Cristianini, N., Demuth, J. P. & Hahn, M. W. CAFE: a computational tool for the study of gene family evolution. *Bioinformatics* **22**, 1269-1271, doi:10.1093/bioinformatics/btl097 (2006).

19 Stamatakis, A. RAxML-VI-HPC: maximum likelihood-based phylogenetic analyses with thousands of taxa and mixed models. *Bioinformatics (Oxford, England)* **22**, 2688-2690, doi:10.1093/bioinformatics/btl446 (2006).

20 Mirarab, S. & Warnow, T. ASTRAL-II: coalescent-based species tree estimation with many hundreds of taxa and thousands of genes. *Bioinformatics* **31**, i44-52, doi:10.1093/bioinformatics/btv234 (2015).

21 Yang, Z. PAML 4: phylogenetic analysis by maximum likelihood. *Mol Biol Evol* **24**, 1586-1591, doi:10.1093/molbev/msm088 (2007).

22 Lupia, R., Lidgard, S. & Crane, P. Comparing palynological abundance and diversity: implications for biotic replacement during the Cretaceous angiosperm radiation. *Paleobiology* **25**, 305-340, doi:10.1017/S009483730002131X (1999).

23 Duplessis, S. *et al.* Obligate biotrophy features unraveled by the genomic analysis of rust fungi. *Proceedings of the National Academy of Sciences of the United States of America* **108**, 9166-9171, doi:10.1073/pnas.1019315108 (2011).

24 Zheng, A. *et al.* The evolution and pathogenic mechanisms of the rice sheath blight pathogen. *Nature Communications* **4**, doi:10.1038/ncomms2427 (2013).

25 Stajich, J. E. *et al.* Insights into evolution of multicellular fungi from the assembled chromosomes of the mushroom Coprinopsis cinerea (Coprinus cinereus). *Proceedings of the National Academy of Sciences of the United States of America* **107**, 11889-11894, doi:10.1073/pnas.1003391107 (2010).

26 Chung, C. L. *et al.* Comparative and population genomic landscape of Phellinus noxius: A hypervariable fungus causing root rot in trees. *Mol Ecol*, doi:10.1111/mec.14359 (2017).

27 Zhang, X. *et al.* Genome-wide high-resolution mapping and functional analysis of DNA methylation in arabidopsis. *Cell* **126**, 1189-1201, doi:10.1016/j.cell.2006.08.003 (2006).

28 Wang, Y. P., Wang, X. Y., Lee, T. H., Mansoor, S. & Paterson, A. H. Gene body methylation shows distinct patterns associated with different gene origins and duplication modes and has a heterogeneous relationship with gene expression in Oryza sativa (rice). *New Phytologist* **198**, 274-283, doi:10.1111/nph.12137 (2013).

950 29 Montanini, B. *et al.* Non-exhaustive DNA methylation-mediated transposon
951 silencing in the black truffle genome, a complex fungal genome with massive
952 repeat element content. *Genome Biol* **15**, 411, doi:10.1186/s13059-014-0411-5
953 (2014).
954 30 Jones, P. A. Functions of DNA methylation: islands, start sites, gene bodies and
955 beyond. *Nat Rev Genet* **13**, 484-492, doi:10.1038/nrg3230 (2012).
956 31 Elango, N., Hunt, B. G., Goodisman, M. A. D. & Yi, S. V. DNA methylation is
957 widespread and associated with differential gene expression in castes of the
958 honeybee, Apis mellifera. *P Natl Acad Sci USA* **106**, 11206-11211,
959 doi:10.1073/pnas.0900301106 (2009).
960 32 Bewick, A. J. *et al.* Diversity of cytosine methylation across the fungal tree of
961 life. *Nat Ecol Evol* **3**, 479-490, doi:10.1038/s41559-019-0810-9 (2019).
962 33 Willing, E. M. *et al.* Genome expansion of Arabis alpina linked with
963 retrotransposition and reduced symmetric DNA methylation. *Nat Plants* **1**,
964 14023, doi:10.1038/nplants.2014.23 (2015).
965 34 Wang, H. *et al.* CG gene body DNA methylation changes and evolution of
966 duplicated genes in cassava. *Proc Natl Acad Sci U S A* **112**, 13729-13734,
967 doi:10.1073/pnas.1519067112 (2015).
968 35 Ma, L. J. *et al.* Comparative genomics reveals mobile pathogenicity
969 chromosomes in Fusarium. *Nature* **464**, 367-373, doi:10.1038/nature08850
970 (2010).
971 36 Deshpande, A. R., Pochapsky, T. C. & Ringe, D. The Metal Drives the
972 Chemistry: Dual Functions of Acireductone Dioxygenase. *Chem Rev* **117**,
973 10474-10501, doi:10.1021/acs.chemrev.7b00117 (2017).
974 37 Dong, S., Raffaele, S. & Kamoun, S. The two-speed genomes of filamentous
975 pathogens: waltz with plants. *Curr Opin Genet Dev* **35**, 57-65,
976 doi:10.1016/j.gde.2015.09.001 (2015).
977 38 Pedersen, B. S. & Quinlan, A. R. Mosdepth: quick coverage calculation for
978 genomes and exomes. *Bioinformatics* **34**, 867-868,
979 doi:10.1093/bioinformatics/btx699 (2018).
980 39 Rokas, A., Wisecaver, J. H. & Lind, A. L. The birth, evolution and death of
981 metabolic gene clusters in fungi. *Nat Rev Microbiol*, doi:10.1038/s41579-018-
982 0075-3 (2018).
983 40 Cortes-Perez, A. *et al.* New species and records of bioluminescent Mycena from
984 Mexico. *Mycologia* **111**, 319-338, doi:10.1080/00275514.2018.1554172 (2019).
985 41 Mihail, J. D. Bioluminescence patterns among North American Armillaria
986 species. *Fungal Biol* **119**, 528-537, doi:10.1016/j.funbio.2015.02.004 (2015).
987 42 Oliveira, A. G. *et al.* Circadian control sheds light on fungal bioluminescence.

988 *Curr Biol* **25**, 964-968, doi:10.1016/j.cub.2015.02.021 (2015).
989 43 Sharpe, M. L., Dearden, P. K., Gimenez, G. & Krause, K. L. Comparative RNA
990 seq analysis of the New Zealand glowworm Arachnocampa luminosa reveals
991 bioluminescence-related genes. *BMC Genomics* **16**, 825, doi:10.1186/s12864-
992 015-2006-2 (2015).
993 44 Fallon, T. R. *et al.* Firefly genomes illuminate parallel origins of
994 bioluminescence in beetles. *Elife* **7**, doi:10.7554/eLife.36495 (2018).
995 45 Desjardin, D. E., Oliveira, A. G. & Stevani, C. V. Fungi bioluminescence
996 revisited. *Photochem Photobiol Sci* **7**, 170-182, doi:10.1039/b713328f (2008).
997 46 Bermudes, D., Petersen, R. H. & Nealson, K. H. Low-Level Bioluminescence
998 Detected in Mycena-Haematopus Basidiocarps. *Mycologia* **84**, 799-802,
999 doi:Doi 10.2307/3760392 (1992).
1000 47 Zhang, B. & Horvath, S. A general framework for weighted gene co-expression
1001 network analysis. *Stat Appl Genet Mol Biol* **4**, Article17, doi:10.2202/1544-
1002 6115.1128 (2005).
1003 48 Langfelder, P. & Horvath, S. WGCNA: an R package for weighted correlation
1004 network analysis. *Bmc Bioinformatics* **9**, 559, doi:10.1186/1471-2105-9-559
1005 (2008).
1006 49 Krizsan, K. *et al.* Transcriptomic atlas of mushroom development reveals
1007 conserved genes behind complex multicellularity in fungi. *Proc Natl Acad Sci*
1008 *U S A* **116**, 7409-7418, doi:10.1073/pnas.1817822116 (2019).
1009 50 Harvey, E. N. *Bioluminescence*. (Academic Press, 1952).
1010 51 Wassink, E. C. in *Bioluminescence in action* (ed P.J. Herring) 171–197
1011 (Academic Press, 1978).
1012 52 Mondego, J. M. *et al.* A genome survey of Moniliophthora perniciosa gives new
1013 insights into Witches' Broom Disease of cacao. *BMC Genomics* **9**, 548,
1014 doi:10.1186/1471-2164-9-548 (2008).
1015 53 Worrall, J. J., Anagnost, S. E. & Zabel, R. A. Comparison of wood decay among
1016 diverse lignicolous fungi. *Mycologia* **89**, 199-219 (1996).
1017 54 Floudas, D. *et al.* The Paleozoic origin of enzymatic lignin decomposition
1018 reconstructed from 31 fungal genomes. *Science* **336**, 1715-1719,
1019 doi:10.1126/science.1221748 (2012).
1020 55 Riley, R. *et al.* Extensive sampling of basidiomycete genomes demonstrates
1021 inadequacy of the white-rot/brown-rot paradigm for wood decay fungi.
1022 *Proceedings of the National Academy of Sciences*,
1023 doi:10.1073/pnas.1400592111 (2014).
1024 56 Miyauchi, S. *et al.* Integrative visual omics of the white-rot fungus Polyporus
1025 brumalis exposes the biotechnological potential of its oxidative enzymes for

1026 delignifying raw plant biomass. *Biotechnol Biofuels* **11**, 201,
1027 doi:10.1186/s13068-018-1198-5 (2018).
1028 57 Marcet-Houben, M. & Gabaldon, T. Evolutionary and functional patterns of
1029 shared gene neighbourhood in fungi. *Nat Microbiol* **4**, 2383-2392,
1030 doi:10.1038/s41564-019-0552-0 (2019).
1031 58 Rincones, J. *et al.* Genetic variability and chromosome-length polymorphisms
1032 of the witches' broom pathogen Crinipellis perniciosa from various plant hosts
1033 in South America. *Mycological Research* **110**, 821-832,
1034 doi:10.1016/j.mycres.2006.05.002 (2006).
1035 59 Zolan, M. E., Heyler, N. K. & Stassen, N. Y. Inheritance of chromosome-length
1036 polymorphisms in Coprinus cinereus. *Genetics* **137**, 87-94 (1994).
1037 60 Moller, M. & Stukenbrock, E. H. Evolution and genome architecture in fungal
1038 plant pathogens. *Nat Rev Microbiol*, doi:10.1038/nrmicro.2017.76 (2017).
1039 61 Zamudio, N. & Bourc'his, D. Transposable elements in the mammalian
1040 germline: a comfortable niche or a deadly trap? *Heredity (Edinb)* **105**, 92-104,
1041 doi:10.1038/hdy.2010.53 (2010).
1042 62 Zemach, A., McDaniel, I. E., Silva, P. & Zilberman, D. Genome-Wide
1043 Evolutionary Analysis of Eukaryotic DNA Methylation. *Science* **328**, 916-919,
1044 doi:10.1126/science.1186366 (2010).
1045 63 Weinstein, P., Delean, S., Wood, T. & Austin, A. D. Bioluminescence in the
1046 ghost fungus Omphalotus nidiformis does not attract potential spore dispersing
1047 insects. *IMA Fungus* **7**, 229-234, doi:10.5598/imafungus.2016.07.02.01 (2016).
1048 64 Purtov, K. V., Petushkov, V. N., Rodionova, N. S. & Gitelson, J. I. Why does the
1049 bioluminescent fungus Armillaria mellea have luminous mycelium but
1050 nonluminous fruiting body? *Dokl Biochem Biophys* **474**, 217-219,
1051 doi:10.1134/S1607672917030176 (2017).
1052 65 Katoh, K. & Standley, D. M. MAFFT multiple sequence alignment software
1053 version 7: improvements in performance and usability. *Molecular biology and*
1054 *evolution* **30**, 772-780, doi:10.1093/molbev/mst010 (2013).
1055 66 Capella-Gutierrez, S., Silla-Martinez, J. M. & Gabaldon, T. trimAl: a tool for
1056 automated alignment trimming in large-scale phylogenetic analyses.
1057 *Bioinformatics* **25**, 1972-1973, doi:10.1093/bioinformatics/btp348 (2009).
1058 67 Nguyen, L. T., Schmidt, H. A., von Haeseler, A. & Minh, B. Q. IQ-TREE: a fast
1059 and effective stochastic algorithm for estimating maximum-likelihood
1060 phylogenies. *Molecular biology and evolution* **32**, 268-274,
1061 doi:10.1093/molbev/msu300 (2015).
1062 68 Hoang, D. T., Chernomor, O., von Haeseler, A., Minh, B. Q. & Vinh, L. S.
1063 UFBoot2: Improving the Ultrafast Bootstrap Approximation. *Molecular*

1064 *biology and evolution* **35**, 518-522, doi:10.1093/molbev/msx281 (2018).
1065 69 Mori, K., Kojima, S., Maki, S., Hirano, T. & Niwa, H. Bioluminescence
1066 characteristics of the fruiting body of Mycena chlorophos. *Luminescence* **26**,
1067 604-610, doi:10.1002/bio.1280 (2011).
1068 70 Shih, Y. S., Chen, C. Y., Lin, W. W. & Kao, H. W. Mycena kentingensis, a new
1069 species of luminous mushroom in Taiwan, with reference to its culture method.
1070 *Mycol Prog* **13**, 429-435, doi:DOI 10.1007/s11557-013-0939-x (2014).
1071 71 Koren, S. *et al.* Canu: scalable and accurate long-read assembly via adaptive k-
1072 mer weighting and repeat separation. *Genome Res* **27**, 722-736,
1073 doi:10.1101/gr.215087.116 (2017).
1074 72 Vaser, R., Sović, I., Nagarajan, N. & Šikić, M. Fast and accurate de novo
1075 genome assembly from long uncorrected reads. *Genome Res* **27**, 737-746,
1076 doi:10.1101/gr.214270.116 (2017).
1077 73 Huang, S., Kang, M. & Xu, A. HaploMerger2: rebuilding both haploid sub-
1078 assemblies from high-heterozygosity diploid genome assembly. *Bioinformatics*,
1079 doi:10.1093/bioinformatics/btx220 (2017).
1080 74 Walker, B. J. *et al.* Pilon: an integrated tool for comprehensive microbial variant
1081 detection and genome assembly improvement. *Plos One* **9**, e112963,
1082 doi:10.1371/journal.pone.0112963 (2014).
1083 75 Benson, G. Tandem repeats finder: a program to analyze DNA sequences.
1084 *Nucleic Acids Res* **27**, 573-580 (1999).
1085 76 Grigoriev, I. V. *et al.* MycoCosm portal: gearing up for 1000 fungal genomes.
1086 *Nucleic Acids Res* **42**, D699-704, doi:10.1093/nar/gkt1183 (2014).
1087 77 Dobin, A. *et al.* STAR: ultrafast universal RNA-seq aligner. *Bioinformatics* **29**,
1088 15-21, doi:10.1093/bioinformatics/bts635 (2013).
1089 78 Dobin, A. & Gingeras, T. R. Mapping RNA-seq Reads with STAR. *Curr Protoc*
1090 *Bioinformatics* **51**, 11 14 11-11 14 19, doi:10.1002/0471250953.bi1114s51
1091 (2015).
1092 79 Haas, B. J. *et al. De novo* transcript sequence reconstruction from RNA-seq
1093 using the Trinity platform for reference generation and analysis. *Nat Protoc* **8**,
1094 1494-1512, doi:10.1038/nprot.2013.084 (2013).
1095 80 Pertea, M. *et al.* StringTie enables improved reconstruction of a transcriptome
1096 from RNA-seq reads. *Nat Biotechnol* **33**, 290-295, doi:10.1038/nbt.3122 (2015).
1097 81 Song, L., Sabunciyan, S. & Florea, L. CLASS2: accurate and efficient splice
1098 variant annotation from RNA-seq reads. *Nucleic Acids Res* **44**, e98,
1099 doi:10.1093/nar/gkw158 (2016).
1100 82 Trapnell, C. *et al.* Differential gene and transcript expression analysis of RNA-
1101 seq experiments with TopHat and Cufflinks. *Nature protocols* **7**, 562-578,

1102 doi:10.1038/nprot.2012.016 (2012).
1103 83 Wu, T. D. & Watanabe, C. K. GMAP: a genomic mapping and alignment
1104 program for mRNA and EST sequences. *Bioinformatics* **21**, 1859-1875,
1105 doi:10.1093/bioinformatics/bti310 (2005).
1106 84 Venturini, L., Caim, S., Kaithakottil, G. G., Mapleson, D. L. & Swarbreck, D.
1107 Leveraging multiple transcriptome assembly methods for improved gene
1108 structure annotation. *GigaScience* **7**, giy093, doi:10.1093/gigascience/giy093
1109 (2018).
1110 85 Stanke, M., Tzvetkova, A. & Morgenstern, B. AUGUSTUS at EGASP: using
1111 EST, protein and genomic alignments for improved gene prediction in the
1112 human genome. *Genome Biol* **7**, S11, doi:10.1186/gb-2006-7-s1-s11 (2006).
1113 86 Ter-Hovhannisyan, V., Lomsadze, A., Chernoff, Y. O. & Borodovsky, M. Gene
1114 prediction in novel fungal genomes using an ab initio algorithm with
1115 unsupervised training. *Genome Research* **18**, 1979-1990,
1116 doi:10.1101/gr.081612.108 (2008).
1117 87 Hoff, K. J., Lange, S., Lomsadze, A., Borodovsky, M. & Stanke, M. BRAKER1:
1118 unsupervised RNA-Seq-Based genome annotation with GeneMark-ET and
1119 AUGUSTUS. *Bioinformatics* **32**, 767-769, doi:10.1093/bioinformatics/btv661
1120 (2016).
1121 88 Korf, I. Gene finding in novel genomes. *BMC Bioinformatics* **5**, 59,
1122 doi:10.1186/1471-2105-5-59 (2004).
1123 89 Conesa, A. *et al.* Blast2GO: a universal tool for annotation, visualization and
1124 analysis in functional genomics research. *Bioinformatics* **21**, 3674-3676,
1125 doi:10.1093/bioinformatics/bti610 (2005).
1126 90 Huerta-Cepas, J. *et al.* Fast genome-wide functional annotation through
1127 orthology assignment by eggNOG-Mapper. *Mol Biol Evol* **34**, 2115-2122,
1128 doi:10.1093/molbev/msx148 (2017).
1129 91 Berriman, M., Coghlan, A. & Jason Tsai, I. J. Creation of a comprehensive
1130 repeat library for a newly sequenced parasitic worm genome. *Protocol*
1131 *Exchange*, doi:10.1038/protex.2018.054 (2018).
1132 92 Ellinghaus, D., Kurtz, S. & Willhoeft, U. LTRharvest, an efficient and flexible
1133 software for de novo detection of LTR retrotransposons. *BMC bioinformatics* **9**,
1134 18, doi:10.1186/1471-2105-9-18 (2008).
1135 93 El-Gebali, S. *et al.* The Pfam protein families database in 2019. *Nucleic Acids*
1136 *Res* **47**, D427-D432, doi:10.1093/nar/gky995 (2019).
1137 94 Smit, A., Hubley, R. & Green, P. *RepeatMasker Open-4.0*. (2013-2015).
1138 95 Quinlan, A. R. & Hall, I. M. BEDTools: a flexible suite of utilities for comparing
1139 genomic features. *Bioinformatics* **26**, 841-842,

1140 doi:10.1093/bioinformatics/btq033 (2010).
1141 96 Price, M. N., Dehal, P. S. & Arkin, A. P. FastTree 2-approximately maximum-
1142 likelihood trees for large alignments. *Plos One* **5**, e9490, doi:ARTN e9490
1143 10.1371/journal.pone.0009490 (2010).
1144 97 Yu, G., Lam, T., Zhu, H. & Guan, Y. Two Methods for Mapping and Visualizing
1145 Associated Data on Phylogeny Using Ggtree. *Molecular Biology and Evolution*
1146 **35**, 3041-3043, doi:10.1093/molbev/msy194 (2018).
1147 98 Guo, W. *et al.* BS-Seeker2: a versatile aligning pipeline for bisulfite sequencing
1148 data. *BMC Genomics* **14**, 774, doi:10.1186/1471-2164-14-774 (2013).
1149 99 Ni, P. *et al.* DeepSignal: detecting DNA methylation state from Nanopore
1150 sequencing reads using deep-learning. *Bioinformatics* **35**, 4586-4595,
1151 doi:10.1093/bioinformatics/btz276 (2019).
1152 100 Conway, J. R., Lex, A. & Gehlenborg, N. UpSetR: an R package for the
1153 visualization of intersecting sets and their properties. *Bioinformatics* **33**, 2938-
1154 2940, doi:10.1093/bioinformatics/btx364 (2017).
1155 101 Yu, G., Smith, D., Zhu, H., Guan, Y. & Lam, T. T. ggtree: an R package for
1156 visualization and annotation of phylogenetic trees with their covariates and
1157 other associated data. *Methods Ecol Evol* **8**, doi:10.1111/2041-210X.12628
1158 (2017).
1159 102 Alexa, A., Rahnenfuhrer, J. & Lengauer, T. Improved scoring of functional
1160 groups from gene expression data by decorrelating GO graph structure.
1161 *Bioinformatics* **22**, 1600-1607, doi:10.1093/bioinformatics/btl140 (2006).
1162 103 Lombard, V., Golaconda Ramulu, H., Drula, E., Coutinho, P. M. & Henrissat,
1163 B. The carbohydrate-active enzymes database (CAZy) in 2013. *Nucleic Acids*
1164 *Res* **42**, D490-495, doi:10.1093/nar/gkt1178 (2014).
1165 104 Buchfink, B., Xie, C. & Huson, D. H. Fast and sensitive protein alignment using
1166 DIAMOND. *Nat Methods* **12**, 59-60, doi:10.1038/nmeth.3176 (2015).
1167 105 Finn, R. D., Clements, J. & Eddy, S. R. HMMER web server: interactive
1168 sequence similarity searching. *Nucleic Acids Res* **39**, W29-37,
1169 doi:10.1093/nar/gkr367 (2011).
1170 106 Kozlov, A., Darriba, D., Flouri, T., Morel, B. & Stamatakis, A. RAxML-NG: a
1171 fast, scalable and user-friendly tool for maximum likelihood phylogenetic
1172 inference. *Bioinformatics* **35**, 4453-4455, doi:10.1093/bioinformatics/btz305
1173 (2019).
1174 107 dos Reis, M. & Yang, Z. Approximate Likelihood Calculation on a Phylogeny
1175 for Bayesian Estimation of Divergence Times. *Molecular Biology and*
1176 *Evolution* **28**, 2161-2172, doi:10.1093/molbev/msr045 (2011).
1177 108 Kumar, S., Stecher, G., Suleski, M. & Hedges, S. B. TimeTree: a resource for

1178 timelines, timetrees, and divergence times. *Mol Biol Evol* **34**, 1812-1819,
1179 doi:10.1093/molbev/msx116 (2017).
1180 109 Poinar, G. & Buckley, R. Evidence of mycoparasitism and
1181 hypermycoparasitism in Early Cretaceous amber. *Mycological Research* **111**,
1182 503-506, doi:10.1016/j.mycres.2007.02.004 (2007).
1183 110 Cai, C., Leschen, R., Hibbett, D., Xia, F. & Huang, D. Mycophagous rove
1184 beetles highlight diverse mushrooms in the Cretaceous. *Nature*
1185 *Communications* **8**, doi:10.1038/ncomms14894 (2017).
1186 111 Guy, L., Kultima, J. R. & Andersson, S. G. genoPlotR: comparative gene and
1187 genome visualization in R. *Bioinformatics* **26**, 2334-2335,
1188 doi:10.1093/bioinformatics/btq413 (2010).
1189 112 Kosakovsky Pond, S. L. *et al.* HyPhy 2.5-A Customizable Platform for
1190 Evolutionary Hypothesis Testing Using Phylogenies. *Molecular biology and*
1191 *evolution* **37**, 295-299, doi:10.1093/molbev/msz197 (2020).
1192 113 Pond, S. L., Frost, S. D. & Muse, S. V. HyPhy: hypothesis testing using
1193 phylogenies. *Bioinformatics* **21**, 676-679, doi:10.1093/bioinformatics/bti079
1194 (2005).
1195 114 Weaver, S. *et al.* Datamonkey 2.0: A Modern Web Application for
1196 Characterizing Selective and Other Evolutionary Processes. *Molecular biology*
1197 *and evolution* **35**, 773-777, doi:10.1093/molbev/msx335 (2018).
1198 115 Delport, W., Poon, A. F., Frost, S. D. & Kosakovsky Pond, S. L. Datamonkey
1199 2010: a suite of phylogenetic analysis tools for evolutionary biology.
1200 *Bioinformatics* **26**, 2455-2457, doi:10.1093/bioinformatics/btq429 (2010).
1201 116 Pond, S. L. & Frost, S. D. Datamonkey: rapid detection of selective pressure on
1202 individual sites of codon alignments. *Bioinformatics* **21**, 2531-2533,
1203 doi:10.1093/bioinformatics/bti320 (2005).
1204 117 Kosakovsky Pond, S. L., Posada, D., Gravenor, M. B., Woelk, C. H. & Frost, S.
1205 D. GARD: a genetic algorithm for recombination detection. *Bioinformatics* **22**,
1206 3096-3098, doi:10.1093/bioinformatics/btl474 (2006).
1207 118 Kosakovsky Pond, S. L. & Frost, S. D. Not so different after all: a comparison
1208 of methods for detecting amino acid sites under selection. *Molecular biology*
1209 *and evolution* **22**, 1208-1222, doi:10.1093/molbev/msi105 (2005).
1210 119 Murrell, B. *et al.* Detecting individual sites subject to episodic diversifying
1211 selection. *Plos Genet* **8**, e1002764, doi:10.1371/journal.pgen.1002764 (2012).
1212 120 Bolger, A. M., Lohse, M. & Usadel, B. Trimmomatic: a flexible trimmer for
1213 Illumina sequence data. *Bioinformatics* **30**, 2114-2120,
1214 doi:10.1093/bioinformatics/btu170 (2014).
1215 121 Liao, Y., Smyth, G. K. & Shi, W. featureCounts: an efficient general purpose

program for assigning sequence reads to genomic features. *Bioinformatics* **30**, 923-930, doi:10.1093/bioinformatics/btt656 (2014).

122 Meinhardt, L. W. *et al.* Genome and secretome analysis of the hemibiotrophic fungal pathogen, Moniliophthora roreri, which causes frosty pod rot disease of cacao: mechanisms of the biotrophic and necrotrophic phases. *BMC Genomics* **15**, 164, doi:10.1186/1471-2164-15-164 (2014).